Imaginal disc growth factors are *Drosophila* Chitinase-like Proteins with roles in morphogenesis and CO_2 response

Authors

Anne Sustar[1], Liesl Strand[1,2] Sandra Zimmerman[1*], Celeste Berg[1*]

[1]Department of Genome Sciences, University of Washington, Seattle, Washington, [2] Current address: Department of Developmental Biology, Stanford University, Stanford, California

***For correspondence**: caberg@uw.edu; sgzim@uw.edu

Abstract

Chitinase-like proteins (CLPs) are members of the family 18 glycosyl hydrolases, which include chitinases and the enzymatically inactive CLPs. A mutation in the enzyme's catalytic site, conserved in vertebrates and invertebrates, allowed CLPs to evolve independently with functions that do not require chitinase activity. CLPs normally function during inflammatory responses, wound healing, and host defense, but when they persist at excessive levels at sites of chronic inflammation and in tissue-remodeling disorders, they correlate positively with disease progression and poor prognosis. However, little is known about their physiological function. *Drosophila melanogaster* has six CLPS, termed Imaginal disc growth factors (Idgfs), encoded by *Idgf1*, *Idgf2*, *Idgf3*, *Idgf4*, *Idgf5*, and *Idgf6*. In this study we developed tools to facilitate characterization of the physiological roles of the Idgfs by deleting each of the *Idgf* genes using the CRISPR/Cas9 system and assessing loss-of-function phenotypes. Using null lines, we showed that loss-of-function for all six Idgf proteins significantly lowers fertility and viability and compromises germ cell migration. We also showed that Idgfs play roles in epithelial morphogenesis, maintaining proper epithelial architecture and cell shape, regulating E-cadherin and cortical Actin, and protecting these tissues against CO_2 exposure. Defining the normal molecular mechanisms of CLPS is key to understanding how deviations tip the balance from a physiological to a pathological state.

Introduction

Chitinase-like proteins (CLPs) are secreted glycoproteins with properties of cytokines and growth factors (Guan *et al.* 2020; Kawamura *et al.* 1999; Kzhyshkowska *et al.* 2016; Lu *et al.* 2022). Normally, CLPs aid in inflammatory responses, wound healing, and defense against parasites, but they also have a dark side (Di Rosa *et al.* 2016; Mazur *et al.* 2021; Pinteac *et al.* 2021; Sutherland *et al.* 2014). Excess levels of CLPs are associated with diseases exhibiting chronically inflamed tissues, such as cancer, asthma, and arthritis, and there they promote the disease process rather than mitigate it (Di Rosa *et al.* 2016; Kzhyshkowska *et al.* 2016; Lee *et al.* 2011; Mazur *et al.* 2021; Pinteac *et al.* 2021; Qureshi *et al.* 2011).

The enzymatically active members of the family 18 glycosyl hydrolases hydrolyze the glycosidic bonds of chitin, a polysaccharide present in plant, fungal, bacterial, and animal species (Fuhrman *et al.* 1992; Miyashita and Fujii 1993; Samac *et al.* 1990; Tharanathan and Kittur 2003; Watanabe *et al.* 1993). CLPs,

on the other hand, lack hydrolytic activity due to substitution of a key amino acid (glutamic acid) in the protein's catalytic domain (e.g., with glutamine in *Drosophila* Idgfs and human CHI3L2, or with leucine in human CHI3L1) (KIRKPATRICK *et al.* 1995; RECKLIES *et al.* 2002; VARELA *et al.* 2002). This mutation was facilitated by duplication of ancestral chitinases, followed by subsequent mutations and further duplications (BUSSINK et al. 2007). Over evolutionary time, CLPs acquired new functions that do not require chitinase activity.

Extensive research in humans has identified four CLPs: chitinase 3 like 1 (CHI3L1), chitinase 3 like 2 (CHI3L2), oviductal glycoprotein 1 (OVGP1), and stabilin-interacting chitinase-like protein (SI-CLP). Most studies have focused on the expression patterns of CLPs and their clinical relevance as potential biomarkers of disease or as targets for therapy (MAZUR *et al.* 2021; PINTEAC *et al.* 2021). Analyses of the associated molecular mechanisms are limited to a few studies identifying binding partners, receptors, or signaling pathways (ARESHKOV *et al.* 2012; FRANCESCONE *et al.* 2011; FUSETTI *et al.* 2003; GUAN *et al.* 2020; HE *et al.* 2013; KZHYSHKOWSKA *et al.* 2004; KZHYSHKOWSKA *et al.* 2006; LIBREROS *et al.* 2013; LOW *et al.* 2015; MALIK *et al.* 2015; SHAO *et al.* 2009; ZHANG *et al.* 2009), but these studies relied on *in vitro* cell culture, binding assays, immunohistochemistry, or biochemical methods rather than whole-animal models. To understand the molecular mechanisms of CLP function in physiological and pathological contexts, we need to analyze function *in vivo,* preferably in a model organism that would allow definitive functional tests.

The six *Drosophila* Idgfs are encoded by genes located at four sites in the genome: *Idgf1*, *Idgf2*, and *Idgf3* are clustered together on the left arm of chromosome 2 (2L), *Idgf4* lies on the X chromosome, while *Idgf5* and *Idgf6* reside ~ 1.7 Mb apart on the right arm of chromosome 2 (2R) (Figure 1A and Table S1) (KAWAMURA *et al.* 1999; KIRKPATRICK *et al.* 1995; ZUROVCOVA AND AYALA 2002). Although now defined with a common nomenclature, the proteins were originally identified through different routes. Idgf6 (previously called DS47) was isolated from media from cultured Schneider line-2 (S2) cells, which have macrophage-like properties (KIRKPATRICK *et al.* 1995). Idgf1, Idgf2, Idgf3, and Idgf4 were isolated from conditioned media from imaginal disc cell culture (Clone 8 cells) (KAWAMURA *et al.* 1999). Idgf5 was identified by computer search of the *Drosophila* genome (ZUROVCOVA AND AYALA 2002).

Idgf proteins exhibit about 50% amino acid identity with each other and 15–25% amino acid sequence homology to family 18 glycosyl hydrolases, which include the chitinases (KAWAMURA *et al.* 1999; VARELA *et al.* 2002). Consistent with their identification as secreted proteins, Idgfs and their human orthologs have an N-terminal signal sequence and an N-linked glycosylation sequence (ARIAS *et al.* 1994; HU *et al.* 1996; KAWAMURA *et al.* 1999; KIRKPATRICK *et al.* 1995; MENG *et al.* 2010; NYIRKOS AND GOLDS 1990; RENKEMA *et al.* 1998; SCHIMPL *et al.* 2012). The proteins form a characteristic barrel structure composed of eight parallel beta sheets surrounded by eight anti-parallel alpha helices (VARELA *et al.* 2002).

Idgfs promote growth, proliferation, polarization, and motility in cultured cells (KAWAMURA *et al.* 1999). They participate in wound healing, protect against infection by nematodes (BROZ *et al.* 2017; KUCEROVA *et al.* 2016), function in detoxification of cells (BROZ *et al.* 2017), and participate in extracellular matrix organization required for molting (PESCH *et al.* 2016). To accomplish these functions, the Idgfs are not co-regulated, but rather, exhibit distinct expression patterns and respond to different stimuli. In the embryo, *Idgf* RNA is localized in cells adjacent to invaginating cells during tissue morphogenesis (KAWAMURA *et al.* 1999). In larvae and adults, Idgfs are expressed by hemocytes and the fat body (functional equivalent of the liver) and secreted into the hemolymph (CARTON AND NAPPI 2001; IRVING *et*

al. 2001; KAWAMURA *et al.* 1999; KHUSH AND LEMAITRE 2000; KIRKPATRICK *et al.* 1995; MEISTER *et al.* 2000). Hemocytes and fat body both participate in innate immune responses. In the ovary, Idgfs are expressed in dynamic patterns specific to the different cell types of the egg chamber (ZIMMERMAN *et al.* 2017). Both over- and under-expression in egg chamber cells disrupt epithelial tube morphogenesis (ESPINOZA AND BERG 2020; ZIMMERMAN *et al.* 2017). Thus, Idgfs function in diverse processes in different tissues.

In this study, we focused on characterizing the physiological roles of the Idgfs by precisely deleting each of the Idgfs using the CRISPR/Cas9 system and assessing the effects of complete loss of function in various tissues and different life stages. We found that flies lacking all six Idgfs have low viability and fertility. Germ cell migration in these mutants is defective and likely contributes to the observed low fertility. We detected numerous cuticle defects in adults, abnormal epithelial morphogenesis in egg chambers, and segmentation defects in embryos. Finally, we found that Idgfs regulate E-cadherin and cortical Actin and protect epithelia against CO_2 exposure.

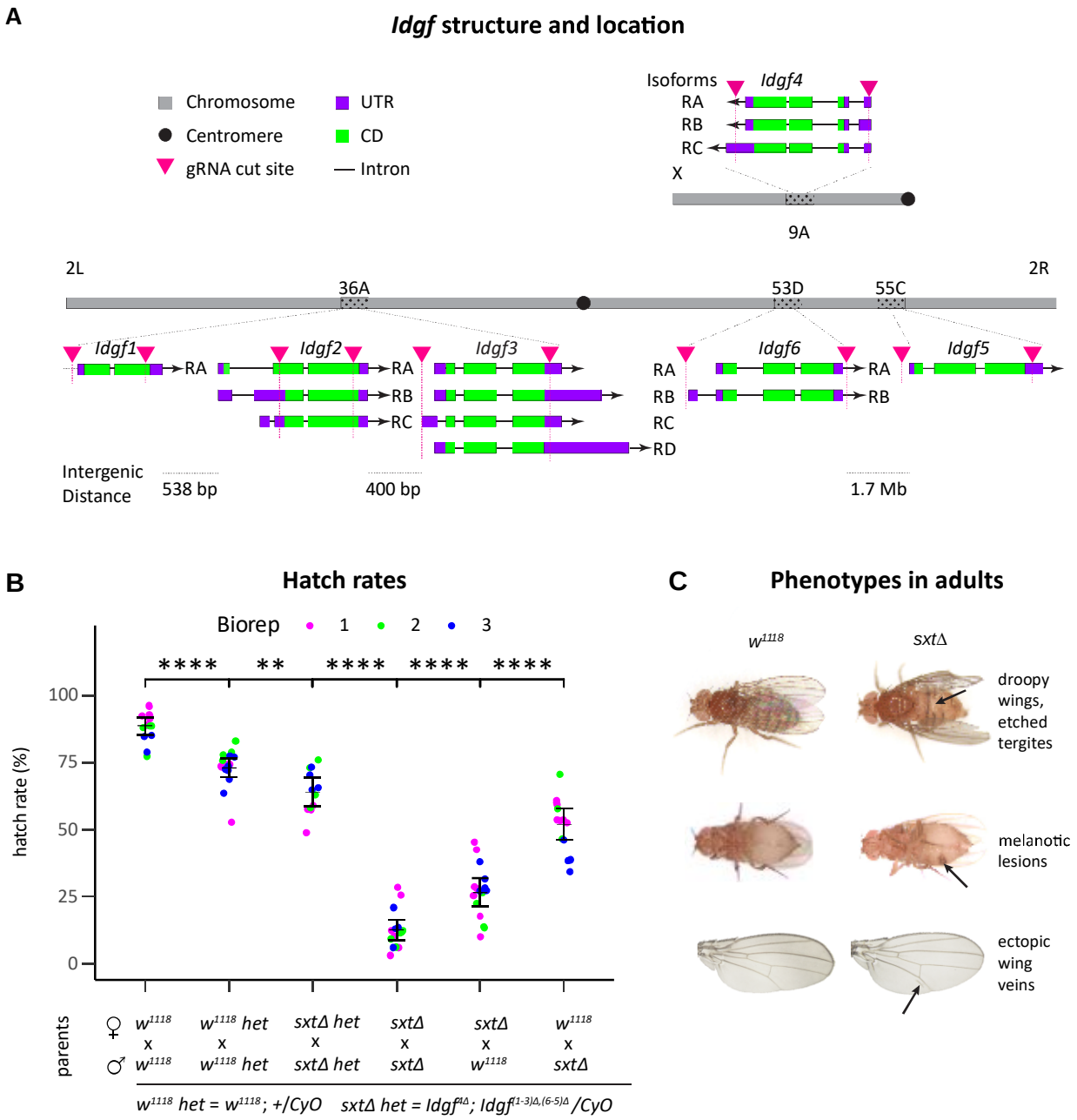

Figure 1 *Idgf* complete knockouts are not entirely lethal. (A) Diagram shows cytological locations of *Idgf* genes and structure of transcript isoforms, including 5' and 3' untranslated regions (purple), coding sequences (green), and introns (thin lines). Black arrows on transcripts indicate the orientation of transcription in the plus (right-pointing) or minus (left-pointing) direction. Arrowheads (magenta) indicate approximate cut sites for deleting each *Idgf* gene. (B) Homozygous and heterozygous *sxtΔ* mutants have low hatch rates relative to control (w^{1118}). Dots represent egg laying assays sampled from three independent biological replicates, ranging from 350-852 eggs analyzed per replicate. Error bars indicate 95% confidence intervals. Significance is based pairwise t-tests with p-values adjusted for multiple comparisons (Benjamini-Hochberg), ** denotes $p \leq 0.01$, ****denotes $p \leq 0.0001$. (C) Adult phenotypes. Top row, dorsal view: etched tergites in adult abdomen (arrow). Wings are held out and down ("droopy" wings). Middle row, ventral view: dark cuticle patches (arrow) are reminiscent of melanotic clots. Bottom row: adult wings display ectopic wing veins (arrow). Anterior is up, distal is to the right.

106 # Results

107 ***Idgf* loss of function phenotypes**

108 To begin to understand how Idgfs function, we developed *Idgf* null lines using the CRISPR/Cas9 system.
109 We precisely deleted the coding region of each *Idgf*, creating single, double, triple, and more mutant
110 lines, as well as a line with all six deletions (w^{1118} $Idgf^{4\Delta}$; $Idgf^{(1-3)\Delta,(6-5)\Delta}$, termed "sextuple mutant" and
111 designated from here on as *sxtΔ*) (Figure 1A, Figure S1, and Table S2). In the laboratory environment of
112 rich food and benign growth conditions, we found no highly penetrant defects in any single mutant.
113 *sxtΔ* flies, however, exhibited numerous phenotypes described below.

114 ***sxtΔ mutants have low viability and fertility***

115 Viability and fertility depend on many developmental processes that require patterning, growth, and cell
116 migration. We assessed the function of Idgfs in this context by quantifying hatch rates for offspring from
117 *sxtΔ* homozygous flies and from *sxtΔ* flies carrying the second chromosome CyO balancer (w^{1118} $Idgf^{4\Delta}$;
118 $Idgf^{(1-3)\Delta,(6-5)\Delta}$/*CyO*). We compared these rates to hatch rates of offspring from w^{1118} and w^{1118} carrying
119 the same second-chromosome balancer (w^{1118}; +/*CyO*) (Figure 1B).

120 The expected hatch rate for offspring from w^{1118}; +/*CyO* parents is 75% of all laid eggs (*CyO/CyO* is
121 lethal). In this background, we observed a hatch rate of 73% compared to a hatch rate of 63% in
122 offspring from w^{1118} $Idgf^{4\Delta}$; $Idgf^{(1-3)\Delta,(6-5)\Delta}$/*CyO* parents. The lower hatch rate for embryos in the *sxtΔ*
123 background indicates that reduction of Idgfs moderately impacts embryonic development. For the
124 heterozygous offspring from this cross (embryos carrying the *CyO* chromosome), maternal and zygotic
125 contributions of wild-type Idgfs comes only from the *CyO* chromosome. In the *sxtΔ* homozygous
126 embryos, all zygotic expression of Idgfs is lost. Consistent with maternal loading of *Idgf* transcripts
127 (Zimmerman et al. 2017), maternal and zygotic loss of Idgfs is more detrimental: nearly 90% of eggs laid
128 by *sxtΔ* females mated to *sxtΔ* males fail to hatch. Surprisingly, some escapers survive to adulthood, and
129 when crossed to w^{1118} flies, these escapers are weakly fertile (Figure 1B).

130 Heterozygous offspring from *sxtΔ* females crossed to w^{1118} males have a higher hatch rate (26.5%) than
131 embryos from a cross between *sxtΔ* homozygotes, presumably due to zygotic expression of wild-type
132 Idgfs, and embryos from w^{1118} females crossed to *sxtΔ* males, which have both maternal and potential
133 zygotic *Idgf* expression in embryos, have a 52% hatch rate (Figure 1B). This percentage is lower than the
134 hatch rate from the $Idgf^{4\Delta}$; $Idgf^{(1-3)\Delta,(6-5)\Delta}$/*CyO* cross, possibly reflecting greater fertility of the male
135 carrying the *CyO* balancer, which expresses wild-type Idgfs. These results indicate that both maternal
136 and zygotic expression of wild-type Idgfs participate in embryonic development.

137 To further explore the effect of loss of Idgfs on viability and development, we compared eclosion rates
138 between homozygous (straight-winged) and heterozygous (curly-winged) adult offspring of
139 heterozygous parents (w^{1118}; +/*CyO* or w^{1118} $Idgf^{4\Delta}$; $Idgf^{(1-3)\Delta,(6-5)\Delta}$/*CyO* males and females). Considering
140 the lethality of homozygous *CyO*/*CyO* flies, the expected Mendelian fractions of curly vs. straight-winged
141 adults should be 2/3 heterozygous (curly-winged) and 1/3 homozyous (straight-winged) flies. Chi-
142 squared analysis demonstrates that the relative fractions in the *sxtΔ* background (73% curly, 27%
143 straight) deviates significantly from the relative fractions of wing phenotypes in the w^{1118} background
144 (69% curly, 31% straight) (p = 0.0087) (Figure S2A). Furthermore, *sxtΔ* homozygotes are
145 developmentally delayed compared to w^{1118} homozygotes. The fraction of *sxtΔ* homozygotes eclosing
146 each day relative to the total after 3 days lags behind the w^{1118} homozygotes (Figure S2B).

147 Taken together, these results indicate that loss of all six Idgfs impacts embryonic development, delays
148 embryonic, larval and/or pupal development, reduces overall adult viability, and lowers both male and
149 female fertility.

150 ***Germ cell migration is defective in sxtΔ***

151 In addition to low hatch rates, *sxtΔ* females laid fewer eggs than control females. Consistent with this
152 observation, ovaries from *sxtΔ* adult females were greatly reduced in size compared to control females.
153 Low fertility in *sxtΔ* flies may be the result of defects in germ cell migration and gonad development.
154 Germ cells form at the posterior pole of the embryo and migrate through the gut, guided by attractive
155 and repellent cues, to the somatic gonadal precursors; together these two cell types form the gonads
156 (BEJSOVEC AND MARTINEZ ARIAS 1991; LEBLANC AND LEHMANN 2017). To assess whether low fertility was a
157 consequence of defects in gonad formation, we marked germ cells with anti-Vasa antibody in control
158 (w^{1118}) and *sxtΔ* embryos (Figure S3A, A'). In the mutants, germ cell number is significantly reduced
159 relative to embryos from control flies (Figure S3B, p=0.0002). These defects potentially involve guidance
160 cues, cell adhesion, or polarization. In support of this hypothesis, we have observed a close association
161 of *Idgf6::GFP* transgene expression with germ cells during embryonic Stages 4-7 (Fig S3C).

162 ***Embryos exhibit segmentation defects***

163 The insect body is organized in a series of segments, regulated by segmentation genes consisting of gap,
164 pair-rule, and segment polarity genes. For example, *engrailed* is a segment polarity gene that is
165 expressed in the posterior two rows of each segment (Figure 4A) and participates in the development of
166 denticle belts (GLOVER AND HAMES 1989, pp.65-66). Denticles are hook-like cuticle structures on the
167 ventral side of each larval segment that provide traction for crawling (Figure S4B). During late
168 embryogenesis, the larval epithelial cells that secrete the ventral cuticle have one of two fates: either
169 they remain smooth, or they produce polarized, actin-based protrusions that form the denticles (DILKS
170 AND DINARDO 2010) (Figure S4C). Maintenance of the segmental pattern of alternating smooth and
171 denticle-producing stripes is regulated by the interactions between Engrailed (En), Wingless (Wg), and
172 Patched (Ptc) (GLOVER AND HAMES 1989, pp. 65-66). The pattern of En expression was disrupted in *sxtΔ*
173 mutant embryos, both on a tissue level and within each cell (Figure S4A',B',C',D'). Smooth cuticle
174 overlapped denticle belts, parts of neighboring belts sometimes fused together, single rows of denticles
175 localized within bands of smooth cuticle, and En aberrantly localized to cell membranes (Figure S4D,D')
176 We explored these defects by examining the segmental pattern of denticle-producing and non-denticle-
177 producing cell shapes in late-stage embryos and discovered an array of altered cell shapes and sizes
178 (Figure 4C,C'). This phenotype could be due to patterning defects, or, alternatively, the cells may have
179 achieved proper cell fate but cannot maintain proper positioning within a segment due to loss of cell-
180 junction integrity. Cell polarity may also be affected.

181 ***Adult flies display a variety of cuticle defects and lesions***

182 Adult *sxtΔ* mutant flies display cuticle defects, i.e., etched tergites and "droopy" wings (Figure 1C, top
183 row). Consistent with the role of Idgfs in immune responses (KUCEROVA *et al.* 2016), adults have lesions
184 resembling melanotic clots, which normally occur at the sites of wounds or at sites of pathogen invasion
185 (Figure 1C, middle row, arrow). Adult wings occasionally have ectopic wing veins (Figure 1C, bottom
186 row, arrow), suggesting defects in wing imaginal-disk patterning during larval and early pupal
187 development.

188 **Overall size of *Idgf* mutant adults was not affected**

189 As noted in the Introduction, CLPs have properties of growth factors (ARESHKOV *et al.* 2012; LEE *et al.*
190 2011; SHAO *et al.* 2009). To assess whether loss of Idgfs compromises growth, we quantified fly size by
191 measuring wing area, which correlates well with overall body size (MIRTH AND SHINGLETON 2012; SIOMAVA
192 *et al.* 2016). We compared wing area in four different genotypes and found no significant difference
193 under our culture conditions. Genotypes: w^{1118}, w^{1118} or $Idgf^{(1-3)\Delta}$ in *trans* to a deficiency generated by
194 the Bloomington Stock Center (NIH P40OD018537) (RYDER *et al.* 2004) that uncovers *Idgf*s 1-3 (Table S3),
195 and $Idgf^{(1-3)\Delta}$ in trans to a wild-type chromosome. We found no significant difference between any of
196 these genotypes under our culture conditions. This result implies that these Idgfs do not contribute to
197 growth and proliferation of imaginal discs and histoblast cells during larval and pupal development.
198 Bristle morphology was also normal.

199 ***Dorsal appendage tube formation is disrupted in sxtΔ mutants***

200 Cell migration, polarization, growth, proliferation, and signaling govern the tissue movements and
201 reconfigurations that form morphologic structures such as epithelial tubes. We used our dorsal
202 appendage (DA) tube morphogenesis model to assess the effects of *Idgf* loss of function during
203 oogenesis (Figure 2A). DA tubes produce eggshell structures that facilitate gas exchange for the
204 developing embryo, and they are made by a subset of follicle cells in late-stage egg chambers. The egg
205 chamber consists of 15 germline-derived nurse cells, one oocyte, and a surrounding monolayer of
206 somatic epithelial cells consisting posteriorly of columnar cells and anteriorly of squamous cells (termed
207 "stretch" cells). The tubes develop from two patches of precursor cells in the follicular epithelium and,
208 through cell intercalation and cell shape change, elongate by migrating anteriorly over the stretch cells
209 and beneath the extracellular matrix (DORMAN *et al.* 2004; OSTERFIELD *et al.* 2013; RITTENHOUSE AND BERG
210 1995; WARD AND BERG 2005). The tube cells secrete eggshell protein into the tube lumen, providing a
211 readout for tube formation, similar to the way a mold forms a sculpture (DAs) (Figure 2A, right image).
212 This highly conserved process of tube formation is a wrapping mechanism akin to mammalian neural
213 tube formation (OSTERFIELD *et al.* 2017).

214 We previously observed disruption of DA morphogenesis using *Idgf1* and *Idgf3* overexpression (ESPINOZA
215 AND BERG 2020; ZIMMERMAN *et al.* 2017) and *Idgf* RNAi for each single mutant (ZIMMERMAN *et al.* 2017).
216 Since null mutations are the gold standard in genetics, we asked "What about complete knockout of
217 *Idgfs*?" We compared the DA phenotypes of eggs laid by each single *Idgf* CRISPR-null mutant and the
218 *sxtΔ* mutant to the DAs of eggs laid by control (w^{1118}) flies and categorized the phenotypes as mild,
219 moderate, or severe by scoring the DAs while blinded to the genotypes (Figure 2B). To limit the
220 influence of potential background mutations, we assessed the phenotypes produced by single mutant
221 genotypes *Idgf1Δ* through *Idgf6Δ* by placing each *Idgf* deletion chromosome *in trans* to a deficiency
222 chromosome generated independently by the Bloomington Stock Center (NIH P40OD018537) (RYDER *et*
223 *al.* 2004). Note that none of the deficiencies produced DA phenotypes on their own (Table S3). The *sxtΔ*
224 mutant was assessed homozygously due to the unfeasibility of creating flies heterozygous with
225 deficiencies spanning each of the six deleted *Idgf* loci.

226 Approximately 50% of eggs laid by the *sxtΔ* mutants and 18% of the *Idgf6*Δ mutants had moderate or
227 severe phenotypes, but both of these percentages varied somewhat from experiment to experiment
228 (see below). The other single mutants (*Idgf1*Δ, *Idgf2*Δ, *Idgf3*Δ, *Idgf4*Δ, and *Idgf5*Δ) did not exhibit

229 significant levels of defects [Figure 2C (i)]. Expression of an *Idgf6::GFP* transgene in a *sxtΔ* mutant
230 background partially rescued the *sxtΔ* DA phenotype [Figure 2C (ii)].

231 Overall, these results provide evidence for important physiologic roles of Idgfs in tissue morphogenesis,
232 potentially including cell polarization, migration, adhesion, and signaling.

233

234

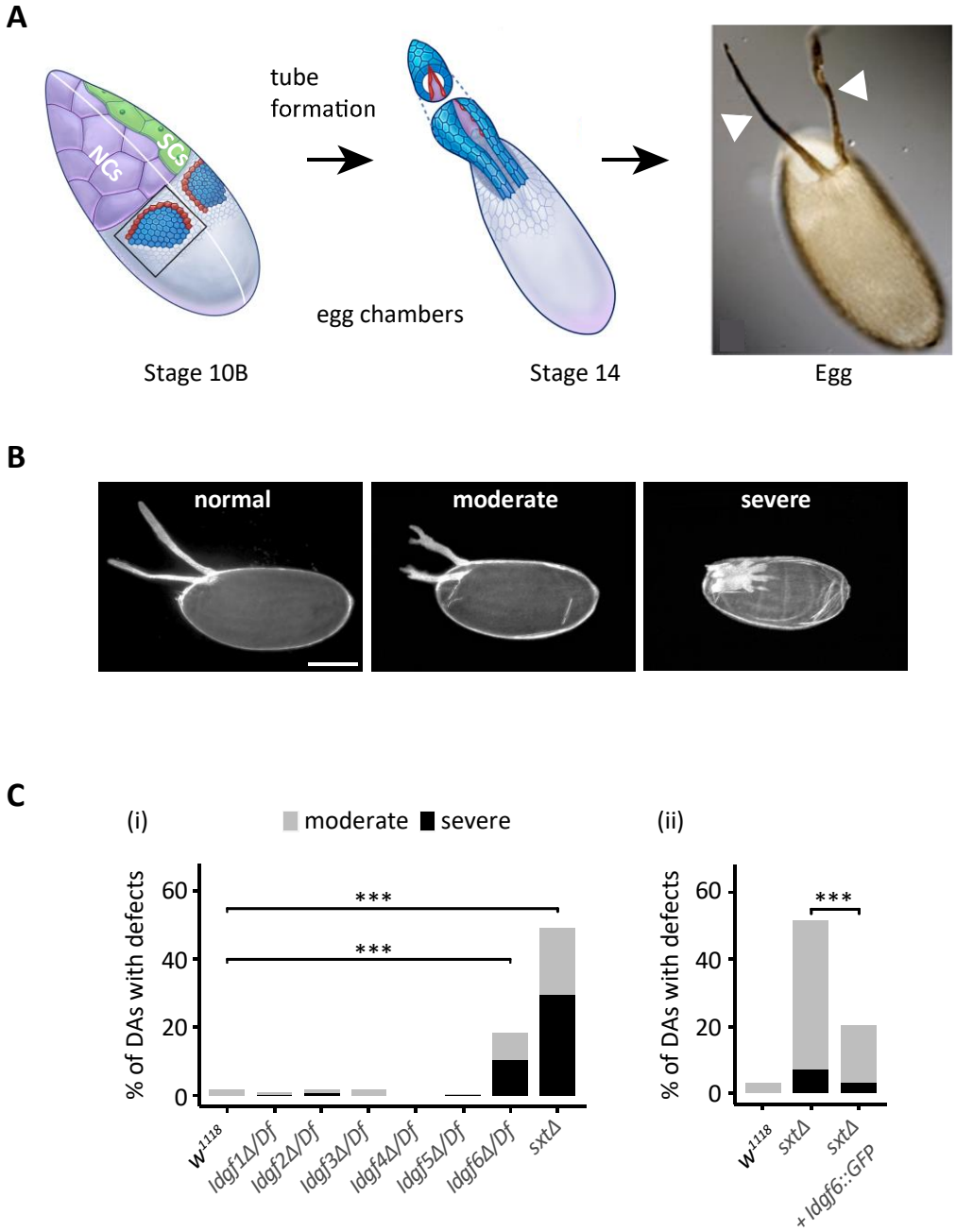

235

236 **Figure 2 Dorsal appendage tube formation and defects in *Idgf* mutants.** (A) Dorsal appendage formation. Roof
237 cells (blue) and floor cells (red) change shape and reorganize to make two DA tubes. Stretch cells (green), cut away
238 to show nurse cells (purple), guide tube elongation. Dorsal appendages (arrowheads) of the laid egg bring air to
239 the embryo that is developing inside the eggshell. (B) Representative examples of DA morphology categorized into
240 normal, moderate, and severe phenotypes. Scale bar = 100µm. (C) Moderate and severe DA phenotypes are
241 significantly increased in eggs laid by *Idgf6*Δ/*Df* and *sxtΔ* females indicating defects in tubulogenesis during
242 oogenesis. *Idgf1*Δ/*Df*, *Idgf2*Δ/*Df*, *Idgf3*Δ/*Df*, *Idgf4*Δ/*Df,* and *Idgf5*Δ/*Df* single mutants do not significantly affect DA
243 morphology [C(i)]. Expression of a wild-type *Idgf6* transgene in *sxtΔ* mutant females partially rescues DA
244 morphology [C(ii)]. Deficiency chromosomes specific to each mutant are listed in Table S3.
245

Idgfs protect against effects of CO_2 exposure

While analyzing the DA defects in eggs laid by *Idgf* mutants, we observed variability in penetrance and expressivity. Initially, we found differences in the percentage and severity of DA defects for eggs laid by *Idgf6Δ* females. Because these two sets of experiments (*Idgf6Δ* vs. other single *Idgf* mutants) were performed by two different lab workers, we asked whether these differences were biological or whether the variability was due to a difference in technique between lab workers (e.g., age of flies, overcrowding, or CO_2 exposure). Intriguingly, we determined that there was variability in whether flies were exposed to CO_2 when they were transferred to fresh egg-laying plates. This observation raised the question as to whether loss of *Idgf* function rendered flies more sensitive to CO_2.

To compare CO_2 sensitivity between wild-type and mutant flies, we assessed DA morphology on eggs laid by w^{1118} flies and *Idgf* mutants by using several different regimes of CO_2 exposure. Treating adult females to 100% CO_2 for 60 seconds twice per day (~every 12 hours) for 3.5 days (Figure S5A) resulted in a significant increase in DA defects on the eggs laid by *Idgf6Δ* and *sxtΔ* mutants, but not on the w^{1118} eggs nor in any of the other single mutants (*Idgf1Δ* through *Idgf5Δ*).

Since tissue and cellular responses to carbon dioxide depend on the length and severity of exposure (HELENIUS *et al.* 2016; HELENIUS *et al.* 2009; SHARABI *et al.* 2009a; SHARABI *et al.* 2009b), we asked if a prolonged exposure to a lower level of CO_2 would have a similar effect. We exposed *sxtΔ* mutant and w^{1118} adult flies to either 20% CO_2 or 100% air and evaluated DA morphology at 1.5 – 2 days and 7-8 days of exposure. Exposure to CO_2 over either of these time periods did not significantly increase DA defects in eggs laid by *sxtΔ* mutants (Figure S5B).

We next asked whether the effect of CO_2 exposure was directly due to the CO_2 itself or due to hypoxia, the transient absence of oxygen. To distinguish between these two hypotheses, we exposed flies to 100% N_2 for five minutes followed by DA analysis at 8 – 10 hours and 2 days after exposure. We did not observe a significant effect on DA morphology following this treatment, indicating that the increase in DA morphology defects was directly due to CO_2 exposure rather than hypoxia (Figure 3A).

These results suggest that Idgf proteins protect tissues against acute CO_2 exposure. If this hypothesis is correct, expression of Idgf protein should rescue the DA mutant phenotype associated with high CO_2. To test this prediction, we used a GFP-tagged transgene, *Idgf6::GFP*, in which Idgf6 is fused in-frame at its C-terminus to superfolder GFP (SAROV *et al.* 2016). We expressed this transgene in the *Idgf6Δ* and *sxtΔ* mutants and compared the DA phenotypes to the same mutants lacking the transgene. We exposed the flies to a single pulse of 100% CO_2 for one minute and analyzed DA defects at 8 – 10 hours and 2 days after exposure (Figure 3B). While both mutants exhibited defects at 8 – 10 hours after exposure, *Idgf6Δ::GFP* expression restored the percentage of DA defects to pre-exposure levels in the *Idgf6Δ* mutants, and it reduced the DA defects in the *sxtΔ* mutants but not to the level of statistical significance. After 2 days, the DA defects in both mutants recovered to pre-exposure levels. These results demonstrate that this gene—environment interaction is due to the loss of Idgfs. Significantly, expression of a single Idgf protein can rescue or ameliorate the DA phenotype in *Idgf* mutants.

To examine the time course following acute CO_2 exposure on a finer scale, we exposed adult *sxtΔ* flies to a single pulse of 100% CO_2 for one minute, followed by hourly DA defect analysis (Figure 3C). Defects peaked at 6 – 10 hours after exposure and then recovered by ~27 hours after exposure.

286 In addition to the developmental roles for Idgfs in normoxia, these results support a hypothesis that
287 Idgfs protect against morphogenetic disruption following acute CO_2 exposure.

288

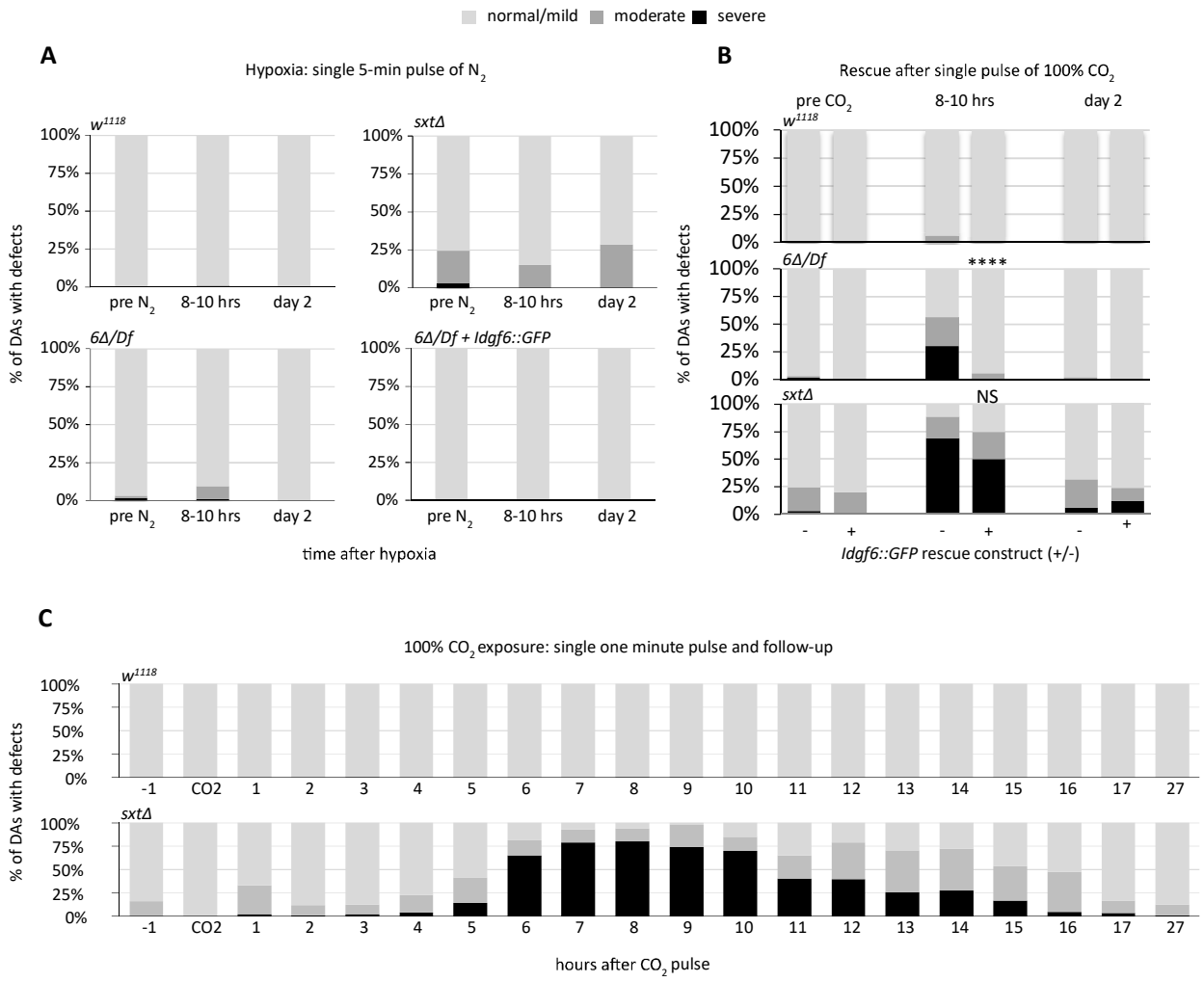

Figure 3 Idgfs protect against CO_2 exposure. (A) Effect of hypoxia on DA phenotype. Air is replaced with 100% N_2 for 5 min to induce hypoxia. DA phenotype is not significantly affected by hypoxia. (B) Expressing a single copy of a wild-type *Idgf6* transgene rescues the DA *Idgf6Δ* phenotype induced by a single, 1-min pulse of 100% CO_2. The sxtΔ phenotype is partially but not significantly rescued (p=0.32). Proportions of defects peak at 8-10 hours after the CO_2 pulse. The *Idgf6Δ* deletion is transheterozygous with a deficiency chromosome to cover potential background mutations. **** denotes significance ($p \leq 0.0001$), NS=not significant. (C) Hourly assessment of DA phenotype following a 1-minute pulse of 100% CO_2. DA defects in eggs laid by *sxtΔ* females peak at 7-10 hours after CO_2 exposure.

299 ***Actin but not E-cadherin is disrupted in egg chambers after CO_2 exposure***

300 How do Idgfs function in DA morphogenesis, and how does acute exposure to CO_2 impact that process?
301 One hypothesis is that Idgfs are necessary for patterning the DA primordial cells. A second hypothesis is
302 that Idgfs regulate cell morphology and epithelial tissue dynamics. To test these hypotheses, we
303 exposed adult females to 100% CO_2 for one minute and then waited for 20-30 minutes before
304 dissecting, fixing, and staining the ovaries. We then examined patterning and cell morphology of the DA-
305 forming cells using antibodies against Broad, a transcription factor that specifies the DA roof-forming
306 cells, and against E-cadherin, an adhesion protein that outlines cell shapes (Dorman et al. 2004; Ward
307 and Berg 2005; Ward et al. 2006).

308 Patterning was normal in both w^{1118} and *sxtΔ* in both the exposed and unexposed egg chambers as
309 revealed by two patches of ~ 50, high-Broad-expressing cells residing just lateral to the dorsal midline
310 (Figure 4A-C). Cell morphology in the DA patches, however, was more disorganized, and E-cadherin was
311 disrupted in the *sxtΔ* exposed egg chambers relative to the exposed w^{1118} and unexposed *sxtΔ* egg
312 chambers (Figure 4A'-C', rectangles). DA cell circumferences were abnormally large in both the exposed
313 and unexposed *sxtΔ* mutants relative to the DA cells in the exposed w^{1118} egg chambers (Figure 4A'-C',
314 rectangles, and Figure 4D-E, rectangles). After exposure to CO_2, *sxtΔ* DA-forming cells were further
315 disrupted by a dramatic loss of Actin from both the cell junctions and the basal surfaces (Figure 4G). In
316 contrast, cell shapes and Actin levels looked normal in the w^{1118} DA-forming cells (Figure 4F).

317

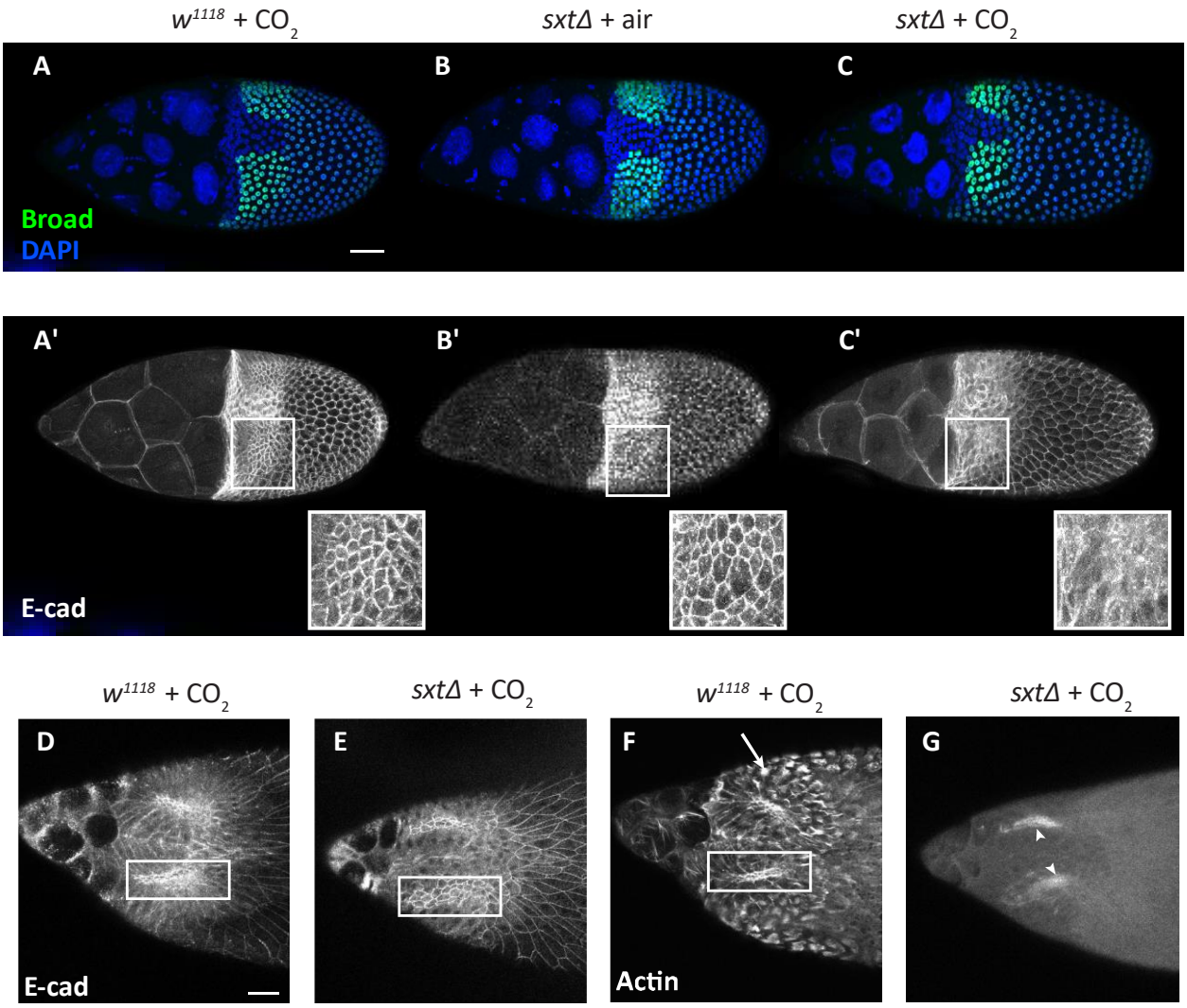

Figure 4 Patterning and cell morphology in DA-forming cells. (A-C') Stage 10B egg chambers. Top row (A-C): Broad (green) marks the roof cells in the DA primordium, DAPI (blue) indicates the nuclei. Patterning is normal in *sxtΔ* mutant exposed to CO_2. Lower row (A'-C'): E-cadherin delineates the apico-lateral cell junctions in follicle cells. Cell morphology is abnormal in *sxtΔ* mutant DAs, and E-cadherin localization is disrupted after a single pulse of 100% CO_2 exposure (white rectangles indicate DA-forming cells). (D-G) Stage 12 egg chambers. DA roof cells (white rectangles) are abnormally large in the *sxtΔ* mutant (E) compared to control (w^{1118}) (D) egg chambers. (F) As shown in w^{1118} egg chambers, basal cell membranes normally exhibit bright spots of Actin localization (arrow). (G) In *sxtΔ* mutants, Actin is lost from cell membranes after CO_2 exposure. Arrowheads in the *sxtΔ* + CO_2 image indicate chorion autofluorescence.

329 We quantified E-cadherin and Actin in the DA-forming follicle cells by measuring fluorescent intensities
330 across cell membranes using ImageJ (Figure 5, Figure S6) and calculating the total area under the plot
331 profiles. To assess whether potential differences in intensity might be stage or cell-type specific, we
332 analyzed roof cells, floor cells, and main-body follicle cells at Stage 10B, just prior to tube wrapping, and
333 at Stage 12, during tube elongation (Figure 5A and Figure S6A). E-cadherin intensity was lower in *sxtΔ*
334 mutants relative to w^{1118} control flies ($p \leq 0.05$), but it was not significantly affected by CO_2 exposure
335 (Figure 5B,C and Figure S6B). In contrast, Actin levels were similar in w^{1118} and *sxtΔ* mutants but
336 dropped quickly in both samples upon exposure to CO_2 ($p \leq 0.05$) (Figure 5B',C' and , Figure S6B'). After
337 30 minutes, Actin intensity recovered in the control egg chambers but remained low in the *sxtΔ* mutant
338 samples (Figure 4F,G). These results suggest that Idgfs regulate E-cadherin expression or stability in
339 normoxia and that they impact Actin dynamics in response to CO_2.

340

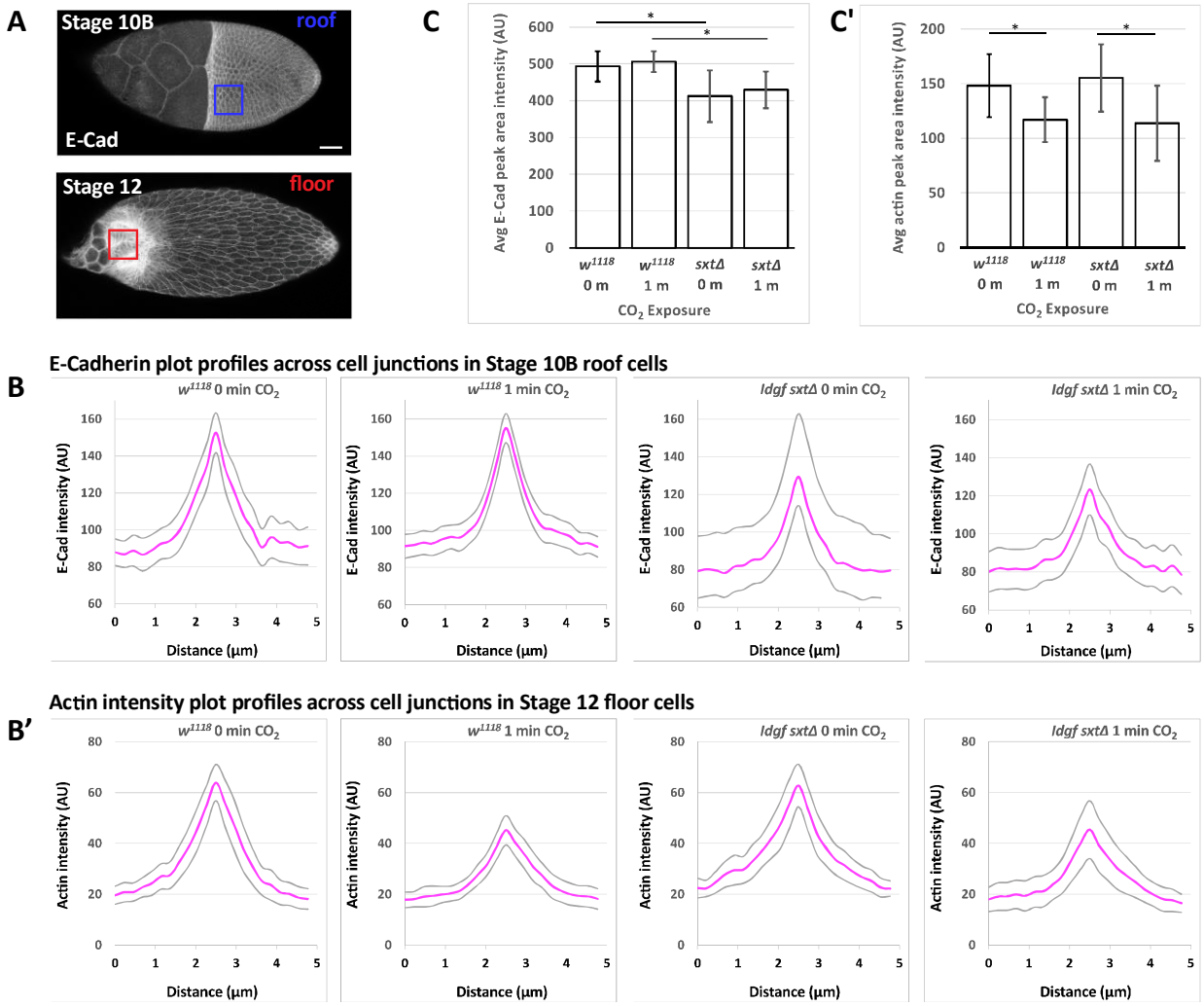

Figure 5 Quantification of cortical Actin and E-Cadherin intensity in DA cells. (A) E-Cadherin and Actin in Stage 10B roof cells (blue square) and Stage 12 floor cells (red square). Scale bar = 50 µm. (B) Comparison of w^{1118} and *sxtΔ* fluorescence intensity plot profiles averaged across three cell membranes, from the center of one cell to the center of the neighboring cell, averaged over at least 6 egg chambers for each genotype and each exposure regime as indicated. Plots show mean (magenta) and confidence limits (gray). (C) Integrated area under the curves in B and B' averaged over all measurements. Error bars show 95% confidence limits. * denotes $p \leq 0.05$, ** denotes $p \leq 0.01$, Student's *t*-test.

350 ***Actin is disrupted in Stage 8-12 embryos after CO_2 exposure***

351 To ask whether Idgfs regulate E-cadherin and Actin in other contexts, we examined E-cadherin and Actin
352 during embryonic development. We exposed w^{1118} and *sxtΔ* embryos of all stages to 100% CO_2 or
353 pressurized air for 2 minutes before de-chorionating, fixing, and staining. Since embryos comprise
354 numerous distinct cell types, we focused on cells near the surface that were relatively uniform in size
355 and easy to measure. We chose ectodermal cells located between the mid-lateral cells and lateral edge
356 of the germ band in abdominal segments 2-6 and measured these cells during the extended germ band
357 stages (late Stage 8 – early Stage 12). Under these conditions, we observed no significant difference
358 between E-cadherin levels in w^{1118} embryos or *sxtΔ* mutant embryos under any of the three conditions
359 (Figure 6A, Figure 6A'). Actin levels also did not differ significantly in w^{1118} embryos between any of the
360 three treatments (Figure 6B, Figure 6B'). However, Actin levels were significantly lower in *sxtΔ* mutants
361 exposed to CO_2 compared to unexposed embryos or embryos exposed to air in either genotype. Taken
362 together, these results support our hypothesis that CO_2 exposure disrupts Actin in embryonic epithelia.

363

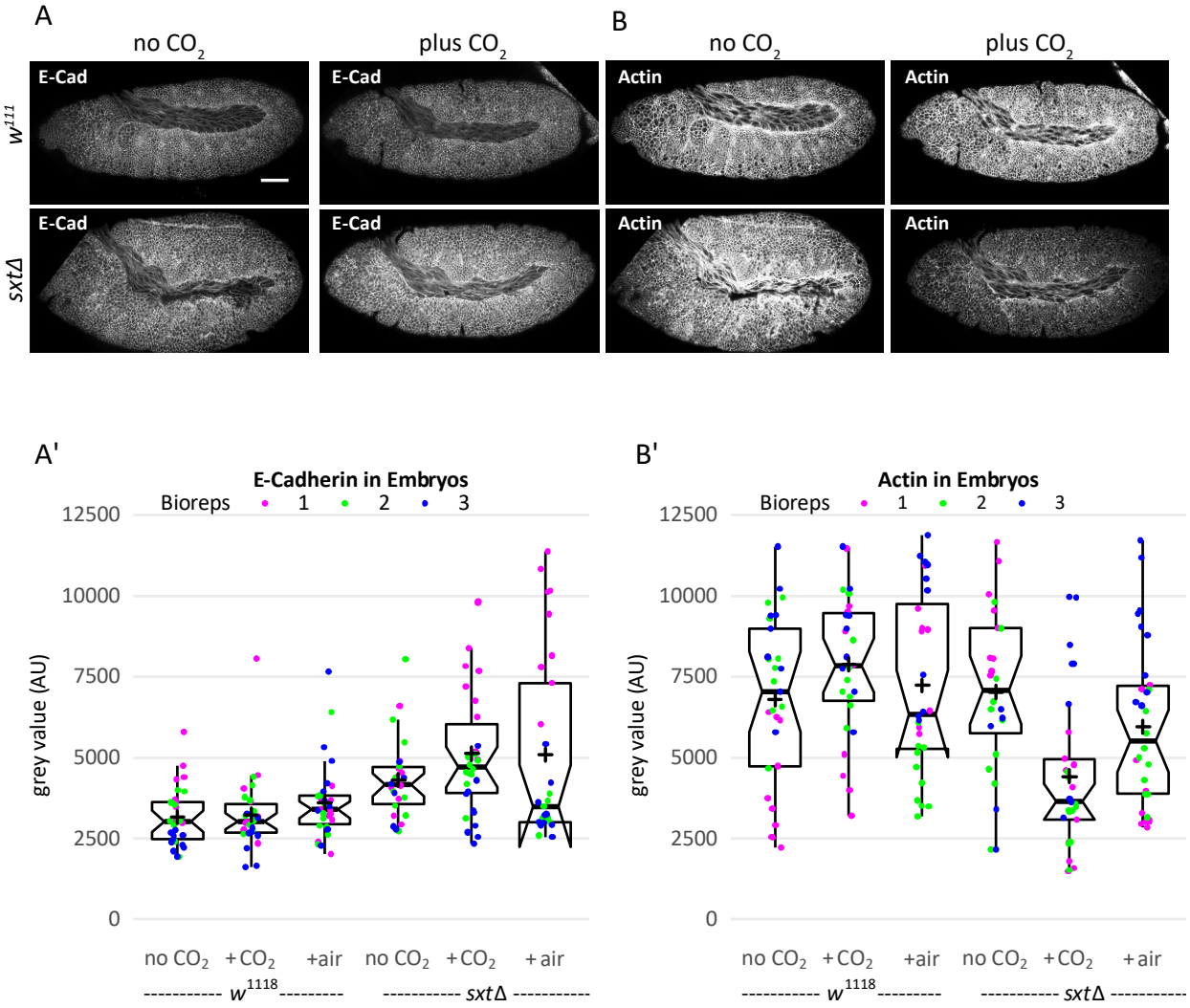

Figure 6 Quantification of cortical Actin and E-Cadherin intensity in Stage 8-12 embryos. (A, B) Representative embryo images showing E-cadherin (A) and Actin (Rhodamine phalloidin) (B) comparing genotypes and CO_2 regime as indicated. Scale bar = 50 µm. (A', B') Comparison of w^{1118} and *sxtΔ* fluorescence intensity measured across 6 cell membranes per embryo, from the center of one cell to the center of the neighboring cell. The colors represent different biological replicates. Each point in the graphs represents the average of the areas under the 6 plot profiles per embryo. The notches on the box plots represent the 95% confidence interval of the medians (horizontal lines), ±1.57*IQR/sqrt(n). IQR = interquartile range. + signs = means. Notches that double back occur when the uncertainty of the median exceeds the IQR. Non-overlapping notches are strong evidence that their medians significantly differ.

377 When analyzing Actin dynamics in egg chambers, we noticed that some cell types were more sensitive
378 to CO_2 exposure than others and that the effect of CO_2 exposure on Actin perdured over a longer period
379 in *sxtΔ* mutants compared to w^{1118} controls. We therefore asked whether we might see more dramatic
380 effects in embryos if we exposed embryos during cellularization, a period when Actin function is crucial
381 (SOKAC *et al.* 2022). We also reasoned that embryonic cells might be protected from CO_2 exposure by
382 the eggshell. We therefore exposed early-stage embryos to 100% CO_2 and increased the exposure time
383 to six minutes. Embryos were allowed to age for 30 minutes before fixing them and staining with
384 phalloidin. We measured Actin fluorescence intensity across cell membranes in syncytial blastoderm
385 embryos during stages 3-5. Prior to cellularization in Stage 5, nuclei in the syncytial blastoderm embryo
386 are surrounded by Actin extensions (called pseudofurrows) at the periphery. In Stage 5, the Actin
387 furrows extend around the nuclei to form a single layer of cells surrounding the yolky core. At these
388 stages, the cells are uniform in size and shape, facilitating uniformity in measurements. As we observed
389 in egg chambers, loss of Actin was significant in early embryos after exposure to CO_2 but did not differ
390 significantly between w^{1118} and *sxtΔ* (Figure 7A,B,C).

391

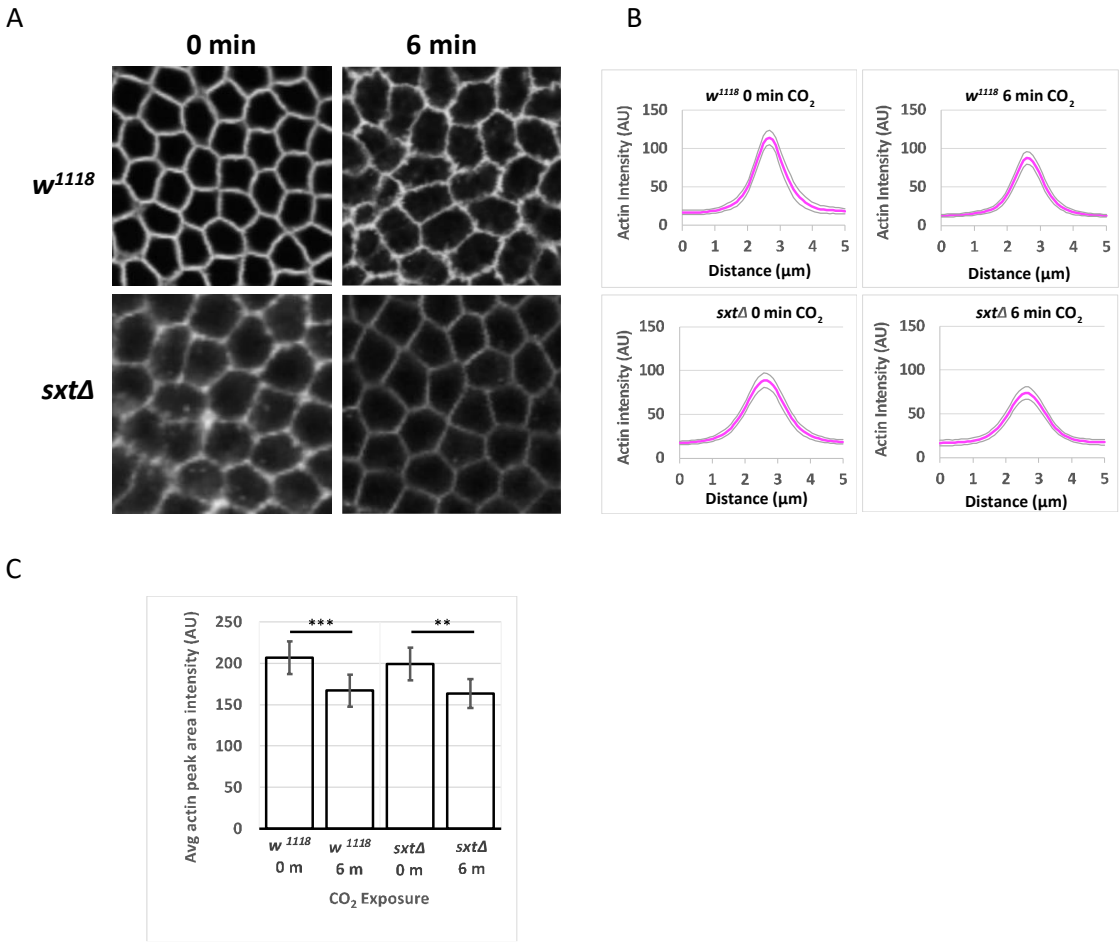

392

393 **Figure 7 Quantification of cortical Actin intensity in Stage 3-5 embryos**. (A) Actin in early embryos comparing
394 genotypes and CO_2 regime as indicated. (B) Comparison of *w*^{1118} and *sxtΔ* fluorescence intensity plot profiles
395 averaged across 6 cell membranes, from the center of one cell to the center of the neighboring cell, averaged over
396 at least 10 Stage 3-5 embryos for each genotype and each exposure regime as indicated. Plots show mean
397 (magenta) and confidence limits (gray). (C) Integrated area under the curves in B averaged over all measurements.
398 Error bars show 95% confidence limits. ** denotes $p \leq 0.01$, *** denotes $p \leq 0.01$, Student's *t*-test.
399

400 # Discussion

401 We investigated the *in vivo* roles of *Drosophila* Imaginal disc growth factors throughout development.
402 Previous studies have sought to characterize the function of individual Idgfs using RNAi or in cell culture.
403 We are the first to delete each of the Idgfs and develop fly lines with single or multiple deletions of the
404 Idgfs, including flies null for all six Idgfs. Using these tools, we found that loss of all Idgf function results
405 in a variety of phenotypes.

406 In *Idgf sxt*Δ mutants, gonads form with significantly reduced germ cell numbers. Most germ cells are
407 lost or die before they reach the somatic gonadal precursor cells, consistent with the low fertility we
408 observed in *sxt*Δ adults. Normally, germ cells form at the anterior pole of the embryo and are taken into
409 the midgut primordium during gastrulation. They initially form a tight cluster in the midgut, but
410 subsequently extend protrusions toward the midgut cells, lose adhesion from each other, disperse,
411 migrate individually through the midgut, and associate with somatic gonadal precursors cells to form the
412 gonads (Review: RICHARDSON AND LEHMANN 2010). To migrate, germ cells become polarized and extend
413 protrusions toward the midgut cells. One hypothesis is that Idgfs participate in remodeling of cell
414 junctions and Actin dynamics in migrating cells, consistent with our finding that loss of all Idgfs disrupts
415 E-cadherin and Actin in certain contexts. A second hypothesis is that loss of Idgf function disrupts
416 polarization and protrusiveness of primordial germ cells, consistent with a previous study demonstrating
417 that Idgfs promote cell motility and protrusiveness in cell culture (KAWAMURA *et al.* 1999). Initial
418 polarization of germ cells requires the G-protein-coupled receptor (GPCR) Trapped in endoderm 1
419 (Tre1), which is expressed in the germ cells and coincides with a redistribution of the Gβ subunit and
420 adherens junction proteins such as Rho1 and E-cadherin (KUNWAR *et al.* 2008). Tre1 is also important for
421 migration across the midgut by signaling through small G proteins and the GTPase Rho1 (KUNWAR *et al.*
422 2003). Studies have identified other key regulators of germ cell migration, such as the lipid phosphate
423 phosphatases, Wunen and Wunen-2 (HANYU-NAKAMURA *et al.* 2004), the small acidic protein, 14-3-3ε
424 (TSIGKARI *et al.* 2012), and pathways such as JAK/STAT (BROWN *et al.* 2006; LI *et al.* 2003). CLPs are known
425 to have properties of cytokines (LEE *et al.* 2011), raising the question of whether Idgfs may promote
426 guidance cues for migrating germ cells. We have observed that Idgf6 associates with migrating germ
427 cells from embryonic Stages 4-7; this association is lost by Stage 10. How Idgfs might interact with these
428 components or otherwise participate in germ cell migration will require further study.

429 Consistent with studies showing expression of Idgfs throughout development, we showed that hatch
430 rates are severely reduced in *sxtΔ* homozygous embryos from *sxtΔ* parents. This effect of loss of all
431 maternal and zygotic Idgfs was ameliorated by adding either maternal, zygotic, or both maternal and
432 zygotically expressed Idgfs. Interestingly, offspring of parents where both parents carry a *CyO*
433 chromosome in a *sxtΔ* background have a higher hatch rate than offspring of w^{1118} females crossed to
434 *sxtΔ* males, even though both scenarios produce embryos that presumably receive both maternal and
435 zygotically expressed Idgfs. Perhaps *sxtΔ* males are less fertile than their *sxtΔ* counterparts carrying the
436 *CyO* chromosome, which expresses wild-type Idgfs. One hypothesis is that the sxtΔ male's fertility is
437 compromised by defective germ cell migration, consistent with our finding that germ cell migration is
438 defective in *sxtΔ* embryos.

439 Further, we found that the proportions of homozygous vs. heterozygous offspring produced by
440 heterozygous parents deviate significantly from the expected Mendelian ratios, reflecting greater
441 lethality of the homozygotes from embryonic through adult stages. Our observation that eclosion is

442 delayed in *sxtΔ* mutants could imply that Idgfs function as growth hormones; loss of function could slow
443 development. Nevertheless, we found no significant size difference between *Idgf* mutants and controls.

444 Consistent with disruption of embryonic development (as revealed by lower *sxtΔ* hatch rates), we
445 observed abnormal expression of Engrailed protein and disorganized denticle belts in embryos, including
446 a mislocalization of Engrailed at the cell membrane. Patterning is achieved through the expression of
447 the segment polarity genes *wingless* (*wg*) and *engrailed* (*en*), which activates expression of *hedgehog*
448 (*hh*). Within each segment, cells receiving the Wg signal produce smooth cuticle posteriorly, and cells
449 receiving the Hh signal produce denticles anteriorly (BEJSOVEC AND MARTINEZ ARIAS 1991; SWARUP AND
450 VERHEYEN 2012). The denticle-versus-smooth cell shapes are distinct: whereas the denticle-producing
451 cells are rectangular and arranged in rows with the long edges oriented in the ventrolateral direction
452 (similar to a staggered brick-wall arrangement), the smooth cells are larger and not arranged in rows
453 (HIRANO *et al.* 2009). Mislocalization or abnormal expression of En could cause a transformation of cell
454 fate from non-denticle-producing to denticle-producing cells, resulting in the disorganized denticle belt
455 phenotype we observed in *sxtΔ* embryos (Figure S4B). Alternatively, cells in the epidermal epithelium
456 may have altered cell adhesion and increased motility, allowing denticle-producing cells to invade into
457 the non-denticle-producing cells.

458 Segmentation defects were apparent in adults in that *sxtΔ* flies exhibited etched tergites. Each
459 abdominal segment in the adult epidermis develops from three bilateral pairs of groups of cells called
460 histoblast nests. The anterior pair in each segment forms the tergite. Histoblast nests proliferate after
461 pupariation and migrate by intercalation into the larval epithelial cells, which then extrude basally and
462 die. The histoblast nests fuse and secrete the adult cuticle (ATHILINGAM *et al.* 2021; DAVIS *et al.* 2022;
463 MANGIONE AND MARTIN-BLANCO 2018; MICHEL AND DAHMANN 2020; NARDI *et al.* 2018; PANZADE AND MATIS
464 2021; PRAT-ROJO *et al.* 2020). Successful migration depends on Decapentaplegic (Dpp) and protrusive
465 extensions at the leading edge of the histoblast nests (NINOV *et al.* 2007; NINOV *et al.* 2010). Our findings
466 suggest a role for Idgfs in cell migration, but how Idgfs function in tergite formation is unknown.

467 Our previous studies showed that the stretch cells relay signals from the nurse cells to the DA cells to
468 guide their movement and ensure tube closure. These signals rely on function of the SOX transcription
469 factor Bullwinkle (Bwk) in the nurse cells [Rittenhouse dissertation, 1996. Bullwinkle, an HMG box
470 protein, is required for proper development during oogenesis, embryogenesis and metamorphosis in
471 *Drosophila melanogaster*, PhD, University of Washington; (RITTENHOUSE AND BERG 1995)], and the non-
472 receptor tyrosine kinases Shark and Src42a in the stretch cells (TRAN AND BERG 2003). The specific
473 signaling molecules and their targets are unknown. *Bwk* mutants produce short, wide, open tubes that
474 create DAs resembling moose antlers (DORMAN *et al.* 2004; RITTENHOUSE AND BERG 1995). Shark and
475 Src42A act downstream of Bwk to regulate DA morphogenesis; Shark loss of function enhances the Bwk
476 phenotype (TRAN AND BERG 2003).

477 In this study, we found that except for *Idgf6*, the single *Idgf*-null mutants did not cause a defective DA
478 phenotype. The results for the single null mutants contrast with our previous studies using RNAi to
479 knock down each *Idgf* individually (ZIMMERMAN *et al.* 2017); we found that RNAi knockdown of each *Idgf*
480 results in a partially penetrant DA phenotype featuring shorter, wider DAs. Shorter, wider DAs also
481 occur when Idgfs are overexpressed or elevated as in eggs from *bwk* mutant flies and contrast with the
482 moderate category of defective DAs in the null mutants, which have thin DAs. Why do significant
483 defects occur in single *Idgf* RNAi knockdowns, but not in single nulls? Functional redundancy from the
484 remaining Idgfs or even from non-Idgf genes could account for the incomplete penetrance or lack of a

485 phenotype. Duplicated genes can maintain functional redundancy despite their divergence over
486 evolutionary time (DEAN *et al.* 2008; DELUNA *et al.* 2008; KAFRI *et al.* 2008; MUSSO *et al.* 2008). Functional
487 redundancy between paralogous genes can result in a strong phenotype when all of the paralogs are
488 deleted and a weak or neutral phenotype when the genes are deleted singly (DEAN *et al.* 2008; DELUNA *et*
489 *al.* 2008; GU *et al.* 2003; KAFRI *et al.* 2008; MUSSO *et al.* 2008), similar to what we observed for the *Idgf*
490 null mutants.

491 Compensation in single null mutants from the remaining wild-type paralogs or even from non-*Idgf* genes
492 could be post-transcriptional, e.g., through increased translation or greater protein stability.
493 Compensation may also occur through transcriptional adaptation, in which upregulation of
494 compensating genes can be triggered by any of a number of mRNA decay pathways that target aberrant
495 mRNAs (GARNEAU *et al.* 2007). A recent study demonstrated that transcriptional adaptation depends on
496 the existence of a mutant mRNA, for which degradation can occur via different surveillance pathways,
497 including non-stop, no-go, or nonsense-mediated decay, depending on the nature of the mutation.
498 Upregulation can then occur in genes with sequence similarity to the degraded mRNA (EL-BROLOSY *et al.*
499 2019; EL-BROLOSY AND STAINIER 2017; GARNEAU *et al.* 2007; ROSSI *et al.* 2015).

500 Except for *Idgf2Δ*, the single null mutants cannot express a transcript. The *Idgf2* deletion leaves intact
501 the 5' UTR, the first exon and intron, and part of the second exon, potentially allowing production of a
502 mutant transcript and therefore transcriptional adaptation in the *Idgf2Δ* and *sxtΔ* mutants, which carry
503 the *Idgf2* deletion. Degradation of the *Idgf2Δ* transcript could not be via the nonsense-mediated decay
504 (NMD) process, which requires a premature stop codon upstream of an intron. Degradation via a non-
505 NMD pathway, however, could be occurring in either the $Idgf^{2\Delta}$ or *sxtΔ* mutant lines. Our RNAi
506 experiments were performed in a wild-type background, so there would be no mutant mRNAs, and any
507 adaptation would be on the translational or post-translational protein level (DELUNA *et al.* 2010;
508 DONNELLY AND STORCHOVA 2014; ISHIKAWA *et al.* 2017; TORRES *et al.* 2008).

509 Although adaptation could be occurring in both the nulls and the knockdowns, the time frame for
510 adaptation could also be a factor. In the RNAi study, we used the GAL4/UAS system to knockdown
511 transcripts from each of the *Idgf* genes. We used a stretch-cell-specific Gal4 driver, which is not
512 expressed until Stage 10 of egg chamber development, after patterning has occurred but just hours
513 before tube formation. This timing may not allow enough time for compensation to occur. On the other
514 hand, *Idgf*-null mutant flies are mutant throughout their entire life cycle. Thus, the different results of
515 our *Idgf* RNAi knockdown and null experiments could be due to different mechanisms of compensation.
516 Discerning whether compensation is occurring and what contributes to the differences in phenotypes
517 exhibited by overexpression, RNAi, and gene deletion will require further study.

518 Mutations can render cells less robust to endogenous or exogenous perturbations (LEVY AND SIEGAL 2008;
519 MASEL AND SIEGAL 2009). *Drosophila* researchers commonly use CO_2 to anesthetize flies without
520 considering the potential profound and long-lasting effects of CO_2 exposure. Previous studies have
521 shown that hypercapnia can suppress the immune system and alter gene expression via the NF-κB
522 pathway in mammalian cells (CUMMINS *et al.* 2010). Hypercapnia also reduces fertility (HELENIUS *et al.*
523 2009) and alters climbing and flight behavior in *Drosophila* (BARTHOLOMEW *et al.* 2015).

524 We demonstrated that exposing *Idgf*-null mutants to CO_2 enhances dorsal appendage morphogenesis
525 defects independently of hypoxia and induces loss of cortical Actin in epithelial tissues during oogenesis
526 and embryonic development. We did note molecular differences, raising the question of whether Idgfs

527 regulate E-cadherin in normoxia and Actin in response to CO_2. We saw that E-cadherin was disrupted in
528 *sxtΔ* mutant egg chambers but was unaffected by CO_2 exposure in either egg chambers or embryos. In
529 contrast, Actin levels were unaffected in *sxtΔ* mutants vs. controls but significantly reduced in *sxtΔ*
530 mutants upon CO_2 exposure. It could be that the Actin is also perturbed in wild-type tissue but recovers,
531 whereas absence of Idgfs eliminates a similar recovery in *sxtΔ* tissue. The mechanisms leading to these
532 novel outcomes are unknown.

533 One possible mechanism for this regulation is that Idgfs interact with the immune deficiency (IMD)
534 pathway through the transcription factor Relish (Drosophila NF-κB). Previous studies show that Relish
535 inhibits JNK signaling (Park et al., 2004). Activation of JNK signaling reorganizes the Actin cytoskeleton,
536 impacting developmental processes such as cell migration and dorsal closure (HOMSY *et al.* 2006; JACINTO
537 *et al.* 2000; KALTSCHMIDT *et al.* 2002; KOCKEL *et al.* 2001; RUDRAPATNA *et al.* 2014). Upon Relish loss, JNK
538 activation causes upregulation of actin remodelers (RAMESH *et al.* 2021). Another possibility is that CO_2
539 exposure reduces pH at the cell membrane, thereby altering Actin dynamics. pH is an important
540 regulator in developmental processes such as differentiation (ULMSCHNEIDER *et al.* 2016) and tissue
541 architecture (GRILLO-HILL *et al.* 2015). Alternatively, the mechanism could involve a pathway
542 independent of JNK signaling or pH.

543 A common thread among the various phenotypes produced by loss of all Idgfs is the disruption of E-
544 cadherin and Actin, an outcome that could interfere with cell migration, segmentation, and tissue
545 morphogenesis. Consistent with this hypothesis, we recently identified eukaryotic translation initiation
546 factor 3 subunit e (eIF3e) as a strong enhancer of Idgf3 overexpression (ESPINOZA AND BERG 2020). eIF3e
547 is part of a complex that regulates the redox enzyme, Mical, which functions to disassemble Actin
548 filaments and inhibit Actin polymerization (GRINTSEVICH *et al.* 2021; GRINTSEVICH *et al.* 2017; GRINTSEVICH *et*
549 *al.* 2016; HUNG *et al.* 2010). We are currently beginning to investigate the mechanistic role of Idgfs in
550 this pathway.

551 Our investigation into the effects of complete loss of function of Idgfs has raised intriguing questions
552 regarding Idgf function. What are the pathways? What are the precise mechanisms? What are the
553 common threads among the various phenotypes? Our *Idgf* null lines are valuable tools that will
554 facilitate studies providing new insights into the function of Idgfs in *Drosophila*. Our results suggest new
555 avenues of investigation for the mechanisms of CLP function in cancer pathogenesis, autoimmune
556 disease, and tissue remodeling disorders.

557

558 Materials and Methods

559 Fly stocks

560 Bloomington stocks: w^{1118} (3605), *Df(2L)ED1102* (24113), *Df(1)ED6989* (9056), *Df(2R)BSC337* (24361),
561 Df(2R)Exel6064 (7546). VDRC stock: Idgf6$^{fTRG01331.sfGFP\text{-}TVPTBF}$ (SAROV *et al.* 2016). Stocks generated in this
562 study: $Idgf^{1\Delta}$, $Idgf^{2\Delta}$, $Idgf^{3\Delta}$, $Idgf^{4\Delta}$, $Idgf^{5\Delta}$, $Idgf^{6\Delta}$, and Idgf$^{4\Delta}$; Idgfp$^{(1\text{-}3)\Delta,(6\text{-}5)\Delta}$ (*sxtΔ*) were used in the
563 experiments. All *Idgf* mutants generated in this study, including double and triple nulls, are listed in
564 Table S2. Flies were maintained on standard molasses food at 25°C.

565 **Reagents and materials**

566 <u>Ovaries</u>

567 - Dissecting dishes and forceps

568 • PBS, 10x (Sambrook et al. 1989), NaCl 80 g, KCl 2 g, Na2HPO4 14.4 g, KH2PO4 2.4 g in 1 L of H2O
569 pH 7.4.
570 • PBT, 0.1% (vol/vol) Tween 20 diluted in 1× PBS
571 • EBR, 10× (modified Ephrussi-Beadle Ringer's solution) 1.3 M NaCl, 47 mM KCl, 19 mM CaCl2 and
572 100 mM HEPES (pH 6.9).
573 • Paraformaldehyde, 4% (wt/vol), Dilute 16% (wt/vol) paraformaldehyde in 1× PBS at a ratio of 1:4
574 • Western Blocking Reagent (WBR)
575
576 Embryos
577 • Flow Buddy - Benchtop Flow Regulator (Genesee Cat #: 59-122B)
578 • Egg collection basket - Falcon tube (50 mL) with the bottom cut off and nylon mesh attached to
579 bottom (e.g., melt the bottom edge slightly with a Bunsen burner and press on the nylon mesh)
580 • Double-sided sticky tape
581 • Whatman paper
582 • Pipette controller (e.g., Millipore Sigma BR25900)
583 • Pasteur pipettes, glass, 3.5 inches
584 • Petri dish lid
585 • Plastic fly bottles punched with holes (to make egg laying chambers when attached to apple
586 juice plates)
587 • 30G syringe needles + plastic syringes
588 • PBTA with 0.05% or 0.1% Triton (1x PBS, 1% BSA, 0.05% or 0.1% Triton X-100, 0.02% Sodium
589 Azide)
590 • Apple juice plates, 175 mL H_2O, 25 mL 4x apple juice, 5 g of agar 1.2 g of methyl paraben. Heat in
591 microwave until agar dissolves. Pour into Petri dish lids. These will be attached to the plastic fly
592 bottles using rubber bands.
593 • Bleach
594 • Heptane Saturated with 37% Formaldehyde - Combine equal volumes of heptane and 37%
595 formaldehyde, shake the mixture vigorously for 15 seconds. Let the solution settle into the 2
596 phases. Prepare the solution the day before it is to be used, shaking the vial or bottle
597 periodically throughout the day. The saturated heptane is the upper phase in the 1:1
598 heptane:formaldehyde stock. Store at room temperature, protected from light, up to several
599 months.
600 • 1x Embryo Wash Solution, - 0.7% NaCl, 0.05% Triton X-100, H_2O
601 • Normal goat serum (NGS)
602
603 **Tissue processing and Immunohistochemistry**

604 Ovaries - Ovaries were dissected in EBR, fixed for 20 minutes in 4% (wt/vol) paraformaldehyde,
605 permeabilized for 1 hour in 1% PBS-Triton, and blocked for 1 hour in WBR. Primary antibodies: mouse
606 anti-Broad (1:500), rat anti-Ecadherin (1:50) (DSHB DCAD2), rabbit anti-Vasa (1:2000) (Paul Lasko)
607 (Figure S2A), rat anti-Vasa (1:500) (Figure S3), mouse anti-Engrailed concentrate (1:20) or supernatant
608 (1:50) (DSHB 4D9). Secondary antibodies: Alexa Fluor goat anti-mouse (1:200) and goat anti-rat (1:200).
609 Ovaries were washed in PBT, incubated O/N at 4°C in PBT with primary antibodies and 5% NGS, washed

610 in PBT, incubated for 1 hour at room temperature in secondary antibodies and DAPI, washed in PBT,
611 mounted on slides and imaged on a Leica SP8X LSM.

612 Embryos - Females were aged for 2 days with wet yeast paste. ~100 males and ~100 females were
613 mated and allowed to lay on apple juice plates O/N or for a few hours to obtain a range of desired
614 stages. All aspects of this experiment prior to dechorionization were done at 25°C. Embryos were
615 exposed to either 100% CO_2 or air for 2 minutes by inserting the CO_2 needle through a hole in the plastic
616 fly bottle. The CO_2 or air was humidified by flowing the gas through a bubbler and the flow rate was
617 held precisely at 3.5 L per minute, using the Flow Buddy. Using a paint brush and embryo wash,
618 embryos were washed from plates into a basket and rinsed with embryo wash using a squirt bottle, then
619 dechorionated in 50% bleach (1:1 bleach:H_2O) for 2 minutes by submerging the mesh end of the basket
620 in a Falcon tube with the bleach. The de-chorionated embryos were rinsed with embryo wash in the
621 basket, then transferred to a 1.5 mL Eppendorf tube by squirting embryo wash onto the outside end of
622 the mesh and into the Eppendorf tube. Embryos were fixed for 40 minutes in 1 mL of heptane saturated
623 with 37% formaldehyde. Using a pipette tip with the tip cut off and pre-treated in PBTA, embryos were
624 transferred to Whatman paper for ~30 seconds to allow the heptane to evaporate. The Whatman paper
625 was placed embryo side down on the tape, gently tapped until embryos were stuck to the tape, and the
626 embryos were immediately covered with PBS. Vitelline membranes were manually removed using 30-
627 Gauge syringe needles. Using a pipette controller attached to a glass Pasteur pipette pre-treated with
628 PBTA, embryos were transferred to PBTA with 0.1% Triton X-100 for staining or to PBTA with 0.05%
629 Triton X-100 for storage at 4°C. Stage 3-5 embryos were incubated with DAPI (1µg/mL), and rhodamine
630 phalloidin (Abcam ab235138) (1:500) for 1 hour, and washed in PBTA with 0.05% Triton X-100 for 1
631 hour, rinsed 3x in PBS, and mounted in Vectashield mounting medium. Stage 8-12 embryos were
632 incubated with rat anti-E-cadherin (1:50) and mouse anti-Engrailed concentrate (1:20) or supernatant
633 (1:50) in PBTA with 0.1% Triton X-100 and NGS O/N at 4°C, washed for 1 hour in PBTA with 0.1% Triton
634 X-100, incubated for 1 hour at RT in PBTA with 0.1% Triton X-100, 5% NGS, DAPI (1µg/mL), rhodamine
635 phalloidin (Abcam ab235138) (1:500), Alexa Fluor goat anti-mouse 488 and anti-rat 647, washed for 1
636 hour in PBTA with 0.1% Triton X-100, rinsed 3x in PBS, and mounted on slides with Vectashield mounting
637 medium.

638 **Generation of *Idgf* mutant fly lines**

639 Deletions of the entire locus or most of the locus for each of *Idgf1*, *Idgf2*, *Idgf3*, *Idgf4*, *Idgf5*, and *Idgf6*
640 were created using CRISPR/Cas9-catalyzed homology-directed repair. For each deletion, we designed
641 and injected three vectors: two guide RNAs and one donor containing a Ds-Red eye reporter to aid in
642 screening newly transformed flies. Using the FlyCRISPR algorithm
643 (tools.flycrispr.molbio.wisc.edu/targetFinder), we designed guide RNAs targeting sites upstream and
644 downstream of each gene. Guide RNAs were synthesized as 5'-phosphorylated oligos (Operon),
645 annealed, and ligated into the BbsI sites of the pU6-BbsI-chiRNA plasmid (Addgene #45946). For the
646 donor vector, we PCR amplified ~1kb homology arms from genomic DNA of the injection strain and
647 cloned them into pHD-DsRed-attP (Addgene #51019). We co-injected guide RNAs and donor vectors
648 (Rainbow Transgenics) into *y vas-Cas9* w^{1118} embryos (Bloomington 55821) and screened F1 flies for
649 germline transmission of the DsRed reporter, followed by single-fly PCR and sequencing. The *Idgf* null
650 strains were outcrossed to w^{1118}*; +; +* for three generations to remove background effects and remove
651 the *vas-Cas9* transgene. All of the single *Idgf*-null lines are homozygous viable and fertile.

652 **Image analysis and quantification**

653 For egg chambers, images were acquired as 8-bit images at the same laser intensities and detector
654 settings on a Leica SP8X LSM. Using ImageJ, we measured E-cadherin and Actin intensity across three
655 cell membranes, from the center of one cell to the center of the neighboring cell, in at least 6 egg
656 chambers for each genotype and compared egg chambers exposed to CO_2 to egg chambers not exposed
657 to CO_2. Plot profiles across 5.0 µm were averaged over all egg chambers for each genotype and
658 treatment.

659 For embryos, images of all genotypes and treatments were acquired as 16-bit images at the same laser
660 intensities and detector settings on a Leica SP8X LSM. For each individual channel and optical plane
661 being measured, background was subtracted, and a median filter was applied (rolling ball radius of 2.0)
662 prior to measurements. For each genotype, we measured E-cadherin and Actin fluorescent intensity as
663 above, across 6 cell membranes per embryo, with n=10 embryos for each treatment (no CO_2, +CO_2, and
664 +air) within three bioreplicates, except for *sxtΔ* bioreplicate 3, no CO_2 (n=6 embryos). Plot profiles across
665 3.5 µm were averaged over all embryos for each genotype and treatment. Total E-cadherin or Actin was
666 calculated by integrating the area under the mean plot profile curve using the trapezoidal rule. Data
667 analyses were performed in Excel. Statistical analyses were performed in Excel and R.

668

669 # Acknowledgements

670 We thank the Bloomington *Drosophila* Stock Center (NIH P40OD018537) and the Vienna *Drosophila*
671 Resource Center for stocks, and FlyBase for genetic, polypeptide, and functional data. The rabbit anti-
672 Vasa antibody (Liu *et al.* 2009) was a gift from Paul Lasko. The mouse anti-Broad, rat anti-Vasa, and rat
673 anti-E-cadherin antibodies were obtained from the Developmental Studies Hybridoma Bank, created by
674 the National Institute of Child Health and Human Development of the National Institutes of Health (NIH)
675 and maintained by the University of Iowa, Department of Biology. We thank Nathaniel Peters at the
676 University of Washington Keck Center for technical support and advice on imaging. We thank Vincent So
677 for providing the data and image for Idgf6::GFP localization to germ cells.

678

679 # Funding

680 NIH R01 GM079433

681 # Author Contributions

682 Celeste Berg – Project design; oversight of all experiments; analysis of mutant embryos; review and
683 editing of manuscript

684 Liesl Strand – Generation of *Idgf6Δ* fly strain using CRISPR/Cas9; experiments and data analysis to
685 examine *Idgf6Δ* dorsal appendage defects; experiments to assess variability in phenotypes; review of
686 manuscript.

687 Anne Sustar – Generation of *Idgf* null fly strains using CRISPR/Cas9; experiments (hatch rates, dorsal
688 appendage morphogenesis, adult phenotype analysis, germ cell migration phenotype, CO_2 response in

689 egg chambers, patterning in egg chambers, Actin and E-cadherin measurements in egg chambers);
690 imaging; data analyses; review of manuscript.

691 Sandra Zimmerman – writing and editing drafts, constructing figures, experiments (E-cadherin and Actin
692 in embryos, hatch rates), imaging, and data analysis.

693

694 Competing Interests

695 The authors declare no competing interests.

696

697 References

698 ARESHKOV, P. O., S. S. AVDIEIEV, O. V. BALYNSKA, D. LEROITH AND V. M. KAVSAN, 2012 Two closely related
699 human members of chitinase-like family, CHI3L1 and CHI3L2, activate ERK1/2 in 293 and U373
700 cells but have the different influence on cell proliferation. Int J Biol Sci **8:** 39-48.
701 ARIAS, E. B., H. G. VERHAGE AND R. C. JAFFE, 1994 Complementary deoxyribonucleic acid cloning and
702 molecular characterization of an estrogen-dependent human oviductal glycoprotein. Biol
703 Reprod **51:** 685-694.
704 ATHILINGAM, T., P. TIWARI, Y. TOYAMA AND T. E. SAUNDERS, 2021 Mechanics of epidermal morphogenesis in
705 the Drosophila pupa. Semin Cell Dev Biol **120:** 171-180.
706 BARTHOLOMEW, N. R., J. M. BURDETT, J. M. VANDENBROOKS, M. C. QUINLAN AND G. B. CALL, 2015 Impaired
707 climbing and flight behaviour in Drosophila melanogaster following carbon dioxide anaesthesia.
708 Sci Rep **5:** 15298.
709 BEJSOVEC, A., AND A. MARTINEZ ARIAS, 1991 Roles of wingless in patterning the larval epidermis of
710 Drosophila. Development **113:** 471-485.
711 BROWN, S., M. P. ZEIDLER AND J. E. HOMBRIA, 2006 JAK/STAT signalling in Drosophila controls cell motility
712 during germ cell migration. Dev Dyn **235:** 958-966.
713 BROZ, V., L. KUCEROVA, L. ROUHOVA, J. FLEISCHMANNOVA, H. STRNAD *et al.*, 2017 Drosophila imaginal disc
714 growth factor 2 is a trophic factor involved in energy balance, detoxification, and innate
715 immunity. Sci Rep **7:** 43273.
716 CARTON, Y., AND A. J. NAPPI, 2001 Immunogenetic aspects of the cellular immune response of Drosophilia
717 against parasitoids. Immunogenetics **52:** 157-164.
718 CUMMINS, E. P., K. M. OLIVER, C. R. LENIHAN, S. F. FITZPATRICK, U. BRUNING *et al.*, 2010 NF-kappaB links CO2
719 sensing to innate immunity and inflammation in mammalian cells. J Immunol **185:** 4439-4445.
720 DAVIS, J. R., A. P. AINSLIE, J. J. WILLIAMSON, A. FERREIRA, A. TORRES-SANCHEZ *et al.*, 2022 ECM degradation in
721 the Drosophila abdominal epidermis initiates tissue growth that ceases with rapid cell-cycle exit.
722 Curr Biol **32:** 1285-1300 e1284.
723 DEAN, E. J., J. C. DAVIS, R. W. DAVIS AND D. A. PETROV, 2008 Pervasive and persistent redundancy among
724 duplicated genes in yeast. PLoS Genet **4:** e1000113.
725 DELUNA, A., M. SPRINGER, M. W. KIRSCHNER AND R. KISHONY, 2010 Need-based up-regulation of protein levels
726 in response to deletion of their duplicate genes. PLoS Biol **8:** e1000347.
727 DELUNA, A., K. VETSIGIAN, N. SHORESH, M. HEGRENESS, M. COLON-GONZALEZ *et al.*, 2008 Exposing the fitness
728 contribution of duplicated genes. Nat Genet **40:** 676-681.
729 DI ROSA, M., G. DISTEFANO, K. ZORENA AND L. MALAGUARNERA, 2016 Chitinases and immunity: Ancestral
730 molecules with new functions. Immunobiology **221:** 399-411.

731 DILKS, S. A., AND S. DINARDO, 2010 Non-cell-autonomous control of denticle diversity in the Drosophila
732 embryo. Development **137:** 1395-1404.
733 DONNELLY, N., AND Z. STORCHOVA, 2014 Dynamic karyotype, dynamic proteome: buffering the effects of
734 aneuploidy. Biochim Biophys Acta **1843:** 473-481.
735 DORMAN, J. B., K. E. JAMES, S. E. FRASER, D. P. KIEHART AND C. A. BERG, 2004 *bullwinkle* is required for
736 epithelial morphogenesis during *Drosophila* oogenesis. Dev Biol **267:** 320-341.
737 EL-BROLOSY, M. A., Z. KONTARAKIS, A. ROSSI, C. KUENNE, S. GUNTHER *et al.*, 2019 Genetic compensation
738 triggered by mutant mRNA degradation. Nature **568:** 193-197.
739 EL-BROLOSY, M. A., AND D. Y. R. STAINIER, 2017 Genetic compensation: A phenomenon in search of
740 mechanisms. PLoS Genet **13:** e1006780.
741 ESPINOZA, C. Y., AND C. A. BERG, 2020 Detecting New Allies: Modifier Screen Identifies a Genetic Interaction
742 Between Imaginal disc growth factor 3 and combover, a Rho-kinase Substrate, During Dorsal
743 Appendage Tube Formation in Drosophila. G3 (Bethesda) **10:** 3585-3599.
744 FRANCESCONE, R. A., S. SCULLY, M. FAIBISH, S. L. TAYLOR, D. OH *et al.*, 2011 Role of YKL-40 in the angiogenesis,
745 radioresistance, and progression of glioblastoma. J Biol Chem **286:** 15332-15343.
746 FUHRMAN, J. A., W. S. LANE, R. F. SMITH, W. F. PIESSENS AND F. B. PERLER, 1992 Transmission-blocking
747 antibodies recognize microfilarial chitinase in brugian lymphatic filariasis. Proc Natl Acad Sci U S
748 A **89:** 1548-1552.
749 FUSETTI, F., T. PIJNING, K. H. KALK, E. BOS AND B. W. DIJKSTRA, 2003 Crystal structure and carbohydrate-
750 binding properties of the human cartilage glycoprotein-39. J Biol Chem **278:** 37753-37760.
751 GARNEAU, N. L., J. WILUSZ AND C. J. WILUSZ, 2007 The highways and byways of mRNA decay. Nat Rev Mol
752 Cell Biol **8:** 113-126.
753 GLOVER, D. M., AND B. D. HAMES, 1989 *Genes and embryos*. IRL Press, Oxford ; New York.
754 GRILLO-HILL, B. K., C. CHOI, M. JIMENEZ-VIDAL AND D. L. BARBER, 2015 Increased H(+) efflux is sufficient to
755 induce dysplasia and necessary for viability with oncogene expression. Elife **4**.
756 GRINTSEVICH, E. E., G. AHMED, A. A. GINOSYAN, H. WU, S. K. RICH *et al.*, 2021 Profilin and Mical combine to
757 impair F-actin assembly and promote disassembly and remodeling. Nat Commun **12:** 5542.
758 GRINTSEVICH, E. E., P. GE, M. R. SAWAYA, H. G. YESILYURT, J. R. TERMAN *et al.*, 2017 Catastrophic disassembly of
759 actin filaments via Mical-mediated oxidation. Nat Commun **8:** 2183.
760 GRINTSEVICH, E. E., H. G. YESILYURT, S. K. RICH, R. J. HUNG, J. R. TERMAN *et al.*, 2016 F-actin dismantling
761 through a redox-driven synergy between Mical and cofilin. Nat Cell Biol **18:** 876-885.
762 GU, Z., L. M. STEINMETZ, X. GU, C. SCHARFE, R. W. DAVIS *et al.*, 2003 Role of duplicate genes in genetic
763 robustness against null mutations. Nature **421:** 63-66.
764 GUAN, R., R. LIN, R. JIN, L. LU, X. LIU *et al.*, 2020 Chitinase-like protein YKL-40 regulates human bronchial
765 epithelial cells proliferation, apoptosis, and migration through TGF-beta1/Smads pathway. Hum
766 Exp Toxicol **39:** 451-463.
767 HANYU-NAKAMURA, K., S. KOBAYASHI AND A. NAKAMURA, 2004 Germ cell-autonomous Wunen2 is required for
768 germline development in Drosophila embryos. Development **131:** 4545-4553.
769 HE, C. H., C. G. LEE, C. S. DELA CRUZ, C. M. LEE, Y. ZHOU *et al.*, 2013 Chitinase 3-like 1 regulates cellular and
770 tissue responses via IL-13 receptor alpha2. Cell Rep **4:** 830-841.
771 HELENIUS, I. T., R. J. HAAKE, Y. J. KWON, J. A. HU, T. KRUPINSKI *et al.*, 2016 Identification of Drosophila Zfh2 as
772 a Mediator of Hypercapnic Immune Regulation by a Genome-Wide RNA Interference Screen. J
773 Immunol **196:** 655-667.
774 HELENIUS, I. T., T. KRUPINSKI, D. W. TURNBULL, Y. GRUENBAUM, N. SILVERMAN *et al.*, 2009 Elevated CO2
775 suppresses specific Drosophila innate immune responses and resistance to bacterial infection.
776 Proc Natl Acad Sci U S A **106:** 18710-18715.
777 HIRANO, M., D. NEFF AND S. COLLIER, 2009 Cell shape and epithelial patterning in the Drosophila embryonic
778 epidermis. Fly (Austin) **3:** 185-191.

779 HOMSY, J. G., H. JASPER, X. G. PERALTA, H. WU, D. P. KIEHART *et al.*, 2006 JNK signaling coordinates integrin
780 and actin functions during Drosophila embryogenesis. Dev Dyn **235:** 427-434.
781 HU, B., K. TRINH, W. F. FIGUEIRA AND P. A. PRICE, 1996 Isolation and sequence of a novel human chondrocyte
782 protein related to mammalian members of the chitinase protein family. J Biol Chem **271:** 19415-
783 19420.
784 HUNG, R.-J., U. YAZDANI, J. YOON, H. WU, T. YANG *et al.*, 2010 Mical links semaphorins to F-actin
785 disassembly. Nature **463:** 823-827.
786 IRVING, P., L. TROXLER, T. S. HEUER, M. BELVIN, C. KOPCZYNSKI *et al.*, 2001 A genome-wide analysis of immune
787 responses in Drosophila. Proc Natl Acad Sci U S A **98:** 15119-15124.
788 ISHIKAWA, K., K. MAKANAE, S. IWASAKI, N. T. INGOLIA AND H. MORIYA, 2017 Post-Translational Dosage
789 Compensation Buffers Genetic Perturbations to Stoichiometry of Protein Complexes. PLoS Genet
790 **13:** e1006554.
791 JACINTO, A., W. WOOD, T. BALAYO, M. TURMAINE, A. MARTINEZ-ARIAS *et al.*, 2000 Dynamic actin-based
792 epithelial adhesion and cell matching during Drosophila dorsal closure. Curr Biol **10:** 1420-1426.
793 KAFRI, R., O. DAHAN, J. LEVY AND Y. PILPEL, 2008 Preferential protection of protein interaction network hubs
794 in yeast: evolved functionality of genetic redundancy. Proc Natl Acad Sci U S A **105:** 1243-1248.
795 KALTSCHMIDT, J. A., N. LAWRENCE, V. MOREL, T. BALAYO, B. G. FERNANDEZ *et al.*, 2002 Planar polarity and actin
796 dynamics in the epidermis of Drosophila. Nat Cell Biol **4:** 937-944.
797 KAWAMURA, K., T. SHIBATA, O. SAGET, D. PEEL AND P. J. BRYANT, 1999 A new family of growth factors produced
798 by the fat body and active on *Drosophila* imaginal disc cells. Development **126:** 211-219.
799 KHUSH, R. S., AND B. LEMAITRE, 2000 Genes that fight infection: what the Drosophila genome says about
800 animal immunity. Trends Genet **16:** 442-449.
801 KIRKPATRICK, R. B., R. E. MATICO, D. E. MCNULTY, J. E. STRICKLER AND M. ROSENBERG, 1995 An abundantly
802 secreted glycoprotein from *Drosophila melanogaster* is related to mammalian secretory proteins
803 produced in rheumatoid tissues and by activated macrophages. Gene **153:** 147-154.
804 KOCKEL, L., J. G. HOMSY AND D. BOHMANN, 2001 Drosophila AP-1: lessons from an invertebrate. Oncogene
805 **20:** 2347-2364.
806 KUCEROVA, L., V. BROZ, B. AREFIN, H. O. MAAROUFI, J. HURYCHOVA *et al.*, 2016 The *Drosophila* chitinase-like
807 protein IDGF3 is involved in protection against nematodes and in wound healing. J Innate
808 Immun **8:** 199-210.
809 KUNWAR, P. S., H. SANO, A. D. RENAULT, V. BARBOSA, N. FUSE *et al.*, 2008 Tre1 GPCR initiates germ cell
810 transepithelial migration by regulating Drosophila melanogaster E-cadherin. J Cell Biol **183:** 157-
811 168.
812 KUNWAR, P. S., M. STARZ-GAIANO, R. J. BAINTON, U. HEBERLEIN AND R. LEHMANN, 2003 Tre1, a G protein-
813 coupled receptor, directs transepithelial migration of Drosophila germ cells. PLoS Biol **1:** E80.
814 KZHYSHKOWSKA, J., A. GRATCHEV, J. H. MARTENS, O. PERVUSHINA, S. MAMIDI *et al.*, 2004 Stabilin-1 localizes to
815 endosomes and the trans-Golgi network in human macrophages and interacts with GGA
816 adaptors. J Leukoc Biol **76:** 1151-1161.
817 KZHYSHKOWSKA, J., S. MAMIDI, A. GRATCHEV, E. KREMMER, C. SCHMUTTERMAIER *et al.*, 2006 Novel stabilin-1
818 interacting chitinase-like protein (SI-CLP) is up-regulated in alternatively activated macrophages
819 and secreted via lysosomal pathway. Blood **107:** 3221-3228.
820 KZHYSHKOWSKA, J., S. YIN, T. LIU, V. RIABOV AND I. MITROFANOVA, 2016 Role of chitinase-like proteins in
821 cancer. Biol Chem **397:** 231-247.
822 LEBLANC, M. G., AND R. LEHMANN, 2017 Domain-specific control of germ cell polarity and migration by
823 multifunction Tre1 GPCR. J Cell Biol **216:** 2945-2958.
824 LEE, C. G., C. A. DA SILVA, C. S. DELA CRUZ, F. AHANGARI, B. MA *et al.*, 2011 Role of chitin and
825 chitinase/chitinase-like proteins in inflammation, tissue remodeling, and injury. Annu Rev
826 Physiol **73:** 479-501.

LEVY, S. F., AND M. L. SIEGAL, 2008 Network hubs buffer environmental variation in Saccharomyces cerevisiae. PLoS Biol **6:** e264.
LI, J., F. XIA AND W. X. LI, 2003 Coactivation of STAT and Ras is required for germ cell proliferation and invasive migration in Drosophila. Dev Cell **5:** 787-798.
LIBREROS, S., R. GARCIA-AREAS, P. KEATING, R. CARRIO AND V. L. IRAGAVARAPU-CHARYULU, 2013 Exploring the role of CHI3L1 in "pre-metastatic" lungs of mammary tumor-bearing mice. Front Physiol **4:** 392.
LIU, N., H. HAN AND P. LASKO, 2009 Vasa promotes Drosophila germline stem cell differentiation by activating mei-P26 translation by directly interacting with a (U)-rich motif in its 3' UTR. Genes Dev **23:** 2742-2752.
LOW, D., R. SUBRAMANIAM, L. LIN, T. AOMATSU, A. MIZOGUCHI *et al.*, 2015 Chitinase 3-like 1 induces survival and proliferation of intestinal epithelial cells during chronic inflammation and colitis-associated cancer by regulating S100A9. Oncotarget **6:** 36535-36550.
LU, Y., N. CHANG, X. ZHAO, R. XUE, J. LIU *et al.*, 2022 Activated Neutrophils Secrete Chitinase-Like 1 and Attenuate Liver Inflammation by Inhibiting Pro-Inflammatory Macrophage Responses. Front Immunol **13:** 824385.
MALIK, P., N. CHAUDHRY, R. MITTAL AND T. K. MUKHERJEE, 2015 Role of receptor for advanced glycation end products in the complication and progression of various types of cancers. Biochim Biophys Acta **1850:** 1898-1904.
MANGIONE, F., AND E. MARTIN-BLANCO, 2018 The Dachsous/Fat/Four-Jointed Pathway Directs the Uniform Axial Orientation of Epithelial Cells in the Drosophila Abdomen. Cell Rep **25:** 2836-2850 e2834.
MASEL, J., AND M. L. SIEGAL, 2009 Robustness: mechanisms and consequences. Trends Genet **25:** 395-403.
MAZUR, M., A. ZIELINSKA, M. M. GRZYBOWSKI, J. OLCZAK AND J. FICHNA, 2021 Chitinases and Chitinase-Like Proteins as Therapeutic Targets in Inflammatory Diseases, with a Special Focus on Inflammatory Bowel Diseases. Int J Mol Sci **22**.
MEISTER, M., C. HETRU AND J. A. HOFFMANN, 2000 The antimicrobial host defense of Drosophila. Curr Top Microbiol Immunol **248:** 17-36.
MENG, G., Y. ZHAO, X. BAI, Y. LIU, T. J. GREEN *et al.*, 2010 Structure of human stabilin-1 interacting chitinase-like protein (SI-CLP) reveals a saccharide-binding cleft with lower sugar-binding selectivity. J Biol Chem **285:** 39898-39904.
MICHEL, M., AND C. DAHMANN, 2020 Tissue mechanical properties modulate cell extrusion in the Drosophila abdominal epidermis. Development **147**.
MIRTH, C. K., AND A. W. SHINGLETON, 2012 Integrating body and organ size in Drosophila: recent advances and outstanding problems. Front Endocrinol (Lausanne) **3:** 49.
MIYASHITA, K., AND T. FUJII, 1993 Nucleotide sequence and analysis of a gene (chiA) for a chitinase from Streptomyces lividans 66. Biosci Biotechnol Biochem **57:** 1691-1698.
MUSSO, G., M. COSTANZO, M. HUANGFU, A. M. SMITH, J. PAW *et al.*, 2008 The extensive and condition-dependent nature of epistasis among whole-genome duplicates in yeast. Genome Res **18:** 1092-1099.
NARDI, J. B., C. M. BEE AND C. L. WALLACE, 2018 Remodeling of the abdominal epithelial monolayer during the larva-pupa-adult transformation of Manduca. Dev Biol **438:** 10-22.
NINOV, N., D. A. CHIARELLI AND E. MARTIN-BLANCO, 2007 Extrinsic and intrinsic mechanisms directing epithelial cell sheet replacement during Drosophila metamorphosis. Development **134:** 367-379.
NINOV, N., S. MENEZES-CABRAL, C. PRAT-ROJO, C. MANJON, A. WEISS *et al.*, 2010 Dpp signaling directs cell motility and invasiveness during epithelial morphogenesis. Curr Biol **20:** 513-520.
NYIRKOS, P., AND E. E. GOLDS, 1990 Human synovial cells secrete a 39 kDa protein similar to a bovine mammary protein expressed during the non-lactating period. Biochem J **269:** 265-268.
OSTERFIELD, M., C. A. BERG AND S. Y. SHVARTSMAN, 2017 Epithelial Patterning, Morphogenesis, and Evolution: Drosophila Eggshell as a Model. Dev Cell **41:** 337-348.

875 OSTERFIELD, M., X. DU, T. SCHUPBACH, E. WIESCHAUS AND S. Y. SHVARTSMAN, 2013 Three-dimensional epithelial
876 morphogenesis in the developing Drosophila egg. Dev Cell **24:** 400-410.
877 PANZADE, S., AND M. MATIS, 2021 The Microtubule Minus-End Binding Protein Patronin Is Required for the
878 Epithelial Remodeling in the Drosophila Abdomen. Front Cell Dev Biol **9:** 682083.
879 PESCH, Y. Y., D. RIEDEL, K. R. PATIL, G. LOCH AND M. BEHR, 2016 Chitinases and Imaginal disc growth factors
880 organize the extracellular matrix formation at barrier tissues in insects. Sci Rep **6:** 18340.
881 PINTEAC, R., X. MONTALBAN AND M. COMABELLA, 2021 Chitinases and chitinase-like proteins as biomarkers in
882 neurologic disorders. Neurol Neuroimmunol Neuroinflamm **8**.
883 PRAT-ROJO, C., P. A. POUILLE, J. BUCETA AND E. MARTIN-BLANCO, 2020 Mechanical coordination is sufficient to
884 promote tissue replacement during metamorphosis in Drosophila. EMBO J **39:** e103594.
885 QURESHI, A. M., A. HANNIGAN, D. CAMPBELL, C. NIXON AND J. B. WILSON, 2011 Chitinase-like proteins are
886 autoantigens in a model of inflammation-promoted incipient neoplasia. Genes Cancer **2:** 74-87.
887 RAMESH, P., N. S. DEY, A. KANWAL, S. MANDAL AND L. MANDAL, 2021 Relish plays a dynamic role in the niche
888 to modulate Drosophila blood progenitor homeostasis in development and infection. Elife **10**.
889 RECKLIES, A. D., C. WHITE AND H. LING, 2002 The chitinase 3-like protein human cartilage glycoprotein 39
890 (HC-gp39) stimulates proliferation of human connective-tissue cells and activates both
891 extracellular signal-regulated kinase- and protein kinase B-mediated signalling pathways.
892 Biochem J **365:** 119-126.
893 RENKEMA, G. H., R. G. BOOT, F. L. AU, W. E. DONKER-KOOPMAN, A. STRIJLAND *et al.*, 1998 Chitotriosidase, a
894 chitinase, and the 39-kDa human cartilage glycoprotein, a chitin-binding lectin, are homologues
895 of family 18 glycosyl hydrolases secreted by human macrophages. Eur J Biochem **251:** 504-509.
896 RICHARDSON, B. E., AND R. LEHMANN, 2010 Mechanisms guiding primordial germ cell migration: strategies
897 from different organisms. Nat Rev Mol Cell Biol **11:** 37-49.
898 RITTENHOUSE, K. R., AND C. A. BERG, 1995 Mutations in the *Drosophila* gene *bullwinkle* cause the formation
899 of abnormal eggshell structures and bicaudal embryos. Development **121:** 3023-3033.
900 ROSSI, A., Z. KONTARAKIS, C. GERRI, H. NOLTE, S. HOLPER *et al.*, 2015 Genetic compensation induced by
901 deleterious mutations but not gene knockdowns. Nature **524:** 230-233.
902 RUDRAPATNA, V. A., E. BANGI AND R. L. CAGAN, 2014 A Jnk-Rho-Actin remodeling positive feedback network
903 directs Src-driven invasion. Oncogene **33:** 2801-2806.
904 RYDER, E., F. BLOWS, M. ASHBURNER, R. BAUTISTA-LLACER, D. COULSON *et al.*, 2004 The DrosDel collection: a set
905 of P-element insertions for generating custom chromosomal aberrations in Drosophila
906 melanogaster. Genetics **167:** 797-813.
907 SAMAC, D. A., C. M. HIRONAKA, P. E. YALLALY AND D. M. SHAH, 1990 Isolation and Characterization of the
908 Genes Encoding Basic and Acidic Chitinase in Arabidopsis thaliana. Plant Physiol **93:** 907-914.
909 SAROV, M., C. BARZ, H. JAMBOR, M. Y. HEIN, C. SCHMIED *et al.*, 2016 A genome-wide resource for the analysis
910 of protein localisation in Drosophila. Elife **5:** e12068.
911 SCHIMPL, M., C. L. RUSH, M. BETOU, I. M. EGGLESTON, A. D. RECKLIES *et al.*, 2012 Human YKL-39 is a pseudo-
912 chitinase with retained chitooligosaccharide-binding properties. Biochem J **446:** 149-157.
913 SHAO, R., K. HAMEL, L. PETERSEN, Q. J. CAO, R. B. ARENAS *et al.*, 2009 YKL-40, a secreted glycoprotein,
914 promotes tumor angiogenesis. Oncogene **28:** 4456-4468.
915 SHARABI, K., A. HURWITZ, A. J. SIMON, G. J. BEITEL, R. I. MORIMOTO *et al.*, 2009a Elevated CO2 levels affect
916 development, motility, and fertility and extend life span in Caenorhabditis elegans. Proc Natl
917 Acad Sci U S A **106:** 4024-4029.
918 SHARABI, K., E. LECUONA, I. T. HELENIUS, G. J. BEITEL, J. I. SZNAJDER *et al.*, 2009b Sensing, physiological effects
919 and molecular response to elevated CO2 levels in eukaryotes. J Cell Mol Med **13:** 4304-4318.
920 SIOMAVA, N., E. A. WIMMER AND N. POSNIEN, 2016 Size relationships of different body parts in the three
921 dipteran species Drosophila melanogaster, Ceratitis capitata and Musca domestica. Dev Genes
922 Evol **226:** 245-256.

923 SOKAC, A. M., N. BIEL AND S. DE RENZIS, 2022 Membrane-actin interactions in morphogenesis: Lessons
924 learned from Drosophila cellularization. Semin Cell Dev Biol.
925 SUTHERLAND, T. E., N. LOGAN, D. RUCKERL, A. A. HUMBLES, S. M. ALLAN *et al.*, 2014 Chitinase-like proteins
926 promote IL-17-mediated neutrophilia in a tradeoff between nematode killing and host damage.
927 Nat Immunol **15:** 1116-1125.
928 SWARUP, S., AND E. M. VERHEYEN, 2012 Wnt/Wingless signaling in Drosophila. Cold Spring Harb Perspect
929 Biol **4**.
930 THARANATHAN, R. N., AND F. S. KITTUR, 2003 Chitin--the undisputed biomolecule of great potential. Crit Rev
931 Food Sci Nutr **43:** 61-87.
932 TORRES, E. M., B. R. WILLIAMS AND A. AMON, 2008 Aneuploidy: cells losing their balance. Genetics **179:** 737-
933 746.
934 TRAN, D. H., AND C. A. BERG, 2003 *bullwinkle* and *shark* regulate dorsal-appendage morphogenesis in
935 *Drosophila* oogenesis. Development **130:** 6273-6282.
936 TSIGKARI, K. K., S. F. ACEVEDO AND E. M. SKOULAKIS, 2012 14-3-3epsilon Is required for germ cell migration in
937 Drosophila. PLoS One **7:** e36702.
938 ULMSCHNEIDER, B., B. K. GRILLO-HILL, M. BENITEZ, D. R. AZIMOVA, D. L. BARBER *et al.*, 2016 Increased
939 intracellular pH is necessary for adult epithelial and embryonic stem cell differentiation. J Cell
940 Biol **215:** 345-355.
941 VARELA, P. F., A. S. LLERA, R. A. MARIUZZA AND J. TORMO, 2002 Crystal structure of imaginal disc growth
942 factor-2. A member of a new family of growth-promoting glycoproteins from *Drosophila*
943 *melanogaster*. J Biol Chem **277:** 13229-13236.
944 VENKEN, K. J., Y. HE, R. A. HOSKINS AND H. J. BELLEN, 2006 P[acman]: a BAC transgenic platform for targeted
945 insertion of large DNA fragments in D. melanogaster. Science **314:** 1747-1751.
946 WARD, E. J., AND C. A. BERG, 2005 Juxtaposition between two cell types is necessary for dorsal appendage
947 tube formation. Mech Dev **122:** 241-255.
948 WATANABE, T., K. KOBORI, K. MIYASHITA, T. FUJII, H. SAKAI *et al.*, 1993 Identification of glutamic acid 204 and
949 aspartic acid 200 in chitinase A1 of Bacillus circulans WL-12 as essential residues for chitinase
950 activity. J Biol Chem **268:** 18567-18572.
951 ZHANG, J., A. GRATCHEV, V. RIABOV, S. MAMIDI, C. SCHMUTTERMAIER *et al.*, 2009 A novel GGA-binding site is
952 required for intracellular sorting mediated by stabilin-1. Mol Cell Biol **29:** 6097-6105.
953 ZIMMERMAN, S. G., G. E. MERRIHEW, M. J. MACCOSS AND C. A. BERG, 2017 Proteomics Analysis Identifies
954 Orthologs of Human Chitinase-Like Proteins as Inducers of Tube Morphogenesis Defects in
955 Drosophila melanogaster. Genetics **206:** 973-984.
956 ZUROVCOVA, M., AND F. J. AYALA, 2002 Polymorphism patterns in two tightly linked developmental genes,
957 Idgf1 and Idgf3, of Drosophila melanogaster. Genetics **162:** 177-188.

958 ## Supplementary Figures and Tables
959
960

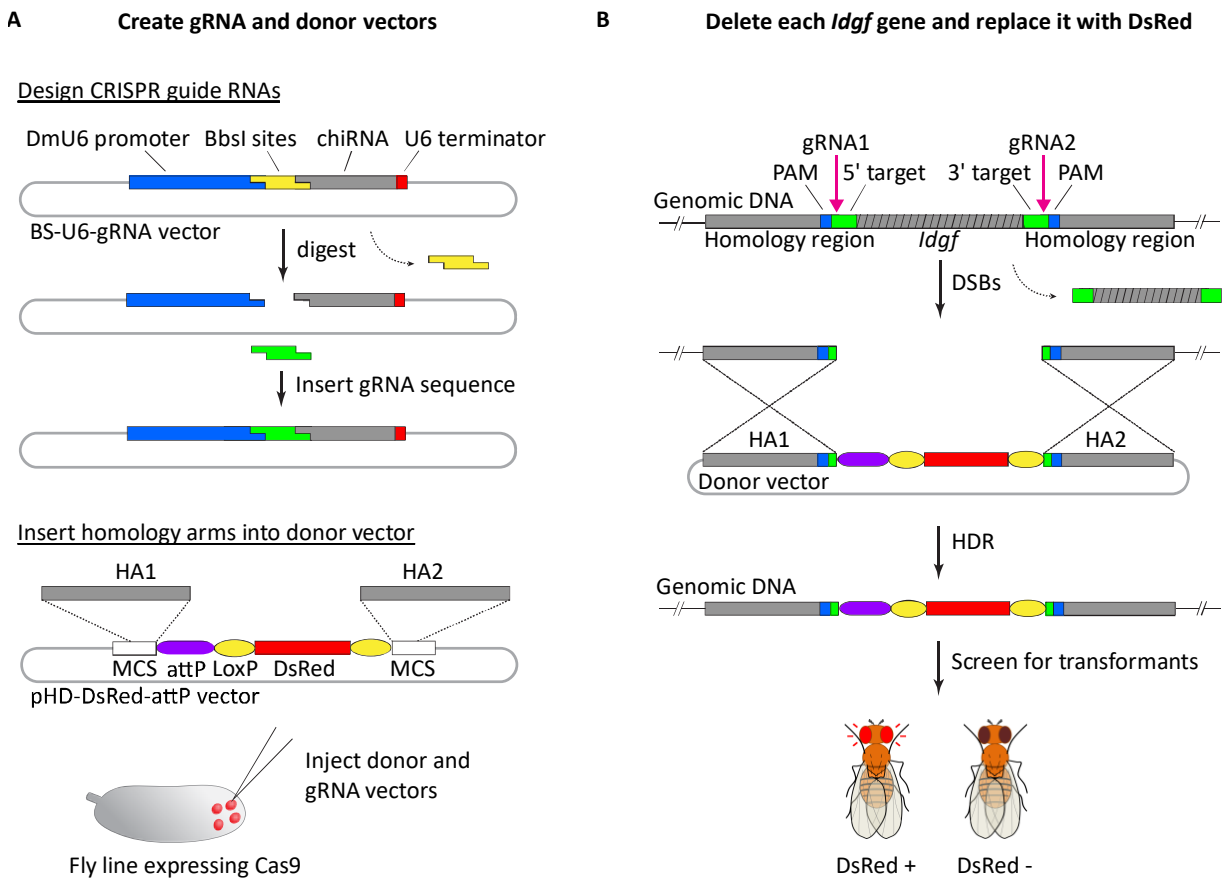

Figure S1 ***Idgf*** **gene deletion method.** (A) Strategy for constructing gRNA vectors and donor vectors for injection into embryos endogenously expressing Cas9. (B) Cas9 exploits gRNAs to make double-strand breaks at sites of pink arrows. Using homology directed repair, the *Idgf* gene is replaced with the gene encoding DsRed fluorescent protein. Transformants are null for the *Idgf* gene of interest and have fluorescent red eyes. gRNA (guide RNA), HA (homology arm), MCS (multiple cloning site) PAM (protospacer adjacent motif), DSB (double-strand break) HDR (homology directed repair).

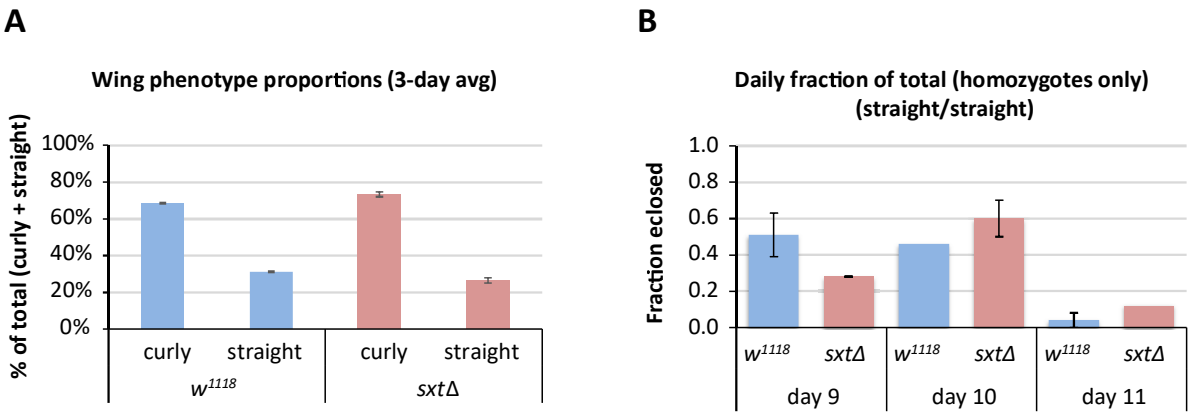

Figure S2 Eclosion rates. (A) Eclosion averaged over 3 days [9-11 days after egg laying (AEL)] for offspring of *+*; *+/CyO* and w^{1118} $Idgf^{4\Delta}$; $Idgf^{(1-3)\Delta,(6-5)\Delta}$/*CyO* crosses. Percentages are the number of curly or straight-winged flies divided by the total (curly + straight). The expected Mendelian fractions of curly vs. straight-winged flies should be 2/3 heterozygous (curly-winged) and 1/3 homozyous (straight-winged) flies. The relative fractions of wing phenotypes in the *sxtΔ* background (73% curly, 27% straight) deviates significantly from the relative fractions in the w^{1118} background (69% curly, 31% straight) (p = 0.0087, X^2 test, n=1304 for the w^{1118} background and 1185 for the *sxtΔ* background). (B) Eclosion rates for homozygous offspring over time. Fractions are the number of homozygous flies eclosed for each day divided by the total number of homozygous flies for all three days. The fraction of w^{1118} homozygotes peaks 1 day earlier than for the *sxtΔ* homozygotes, indicating that the *sxtΔ* homozygotes are developmentally delayed.

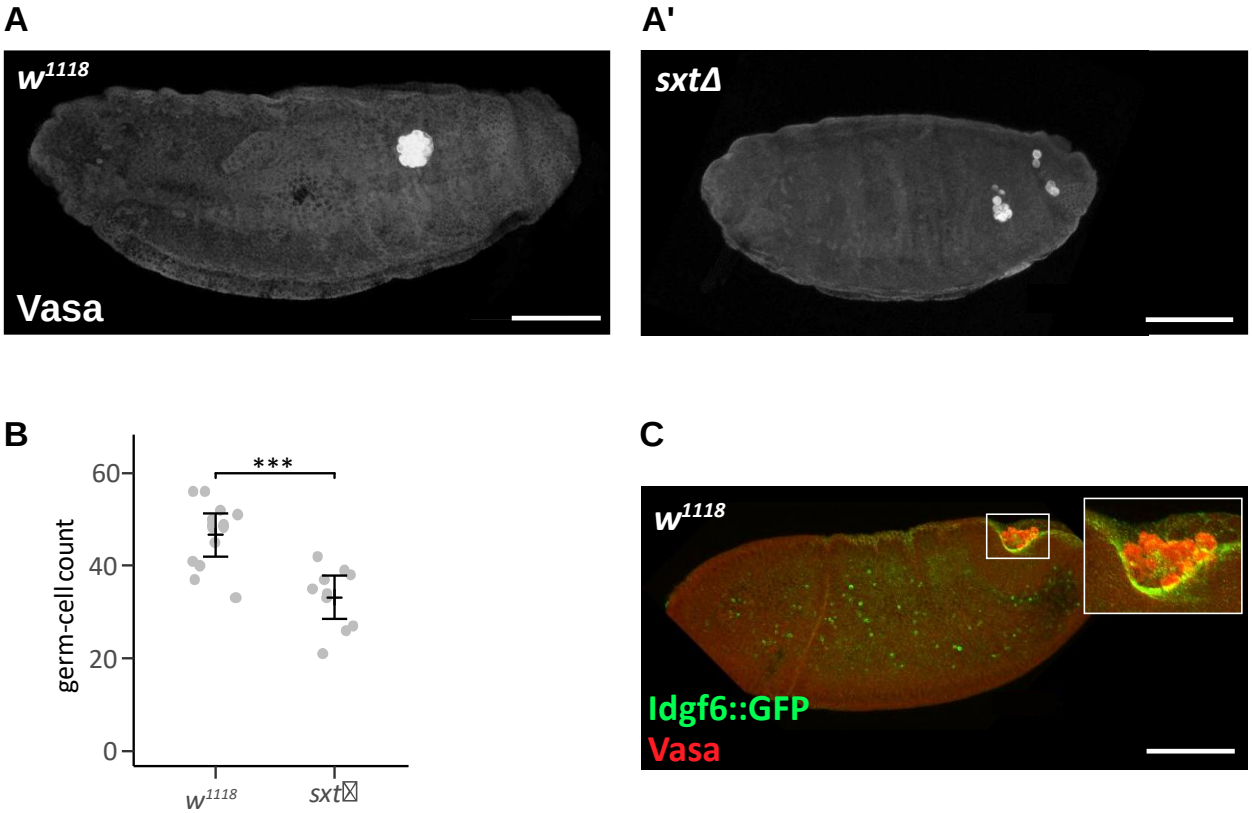

Figure S3 Germ cell migration. Anterior is to the left, dorsal is up in A, A', and C. (A, A') Germ cells in 16-hour old embryos are marked with anti-Vasa antibody, revealing germ-cell loss and reduced numbers in the gonads of sxtΔ versus w^{1118} embryos. Scale bar = 50µm. (B) Graph shows germ cell counts in individual 3-hour old cellular blastoderm embryos. w^{1118}, mean = 46.6 (n= 12 embryos), *sxtΔ*, mean = 33.2 (n= 10 embryos), $p = 0.0002$, Student's *t*-test. (C) During germband extension, GFP-tagged Idgf6 (green) is present in and around the pole cells, which are marked with anti-Vasa antibody (red). Scale bars = 100µm.

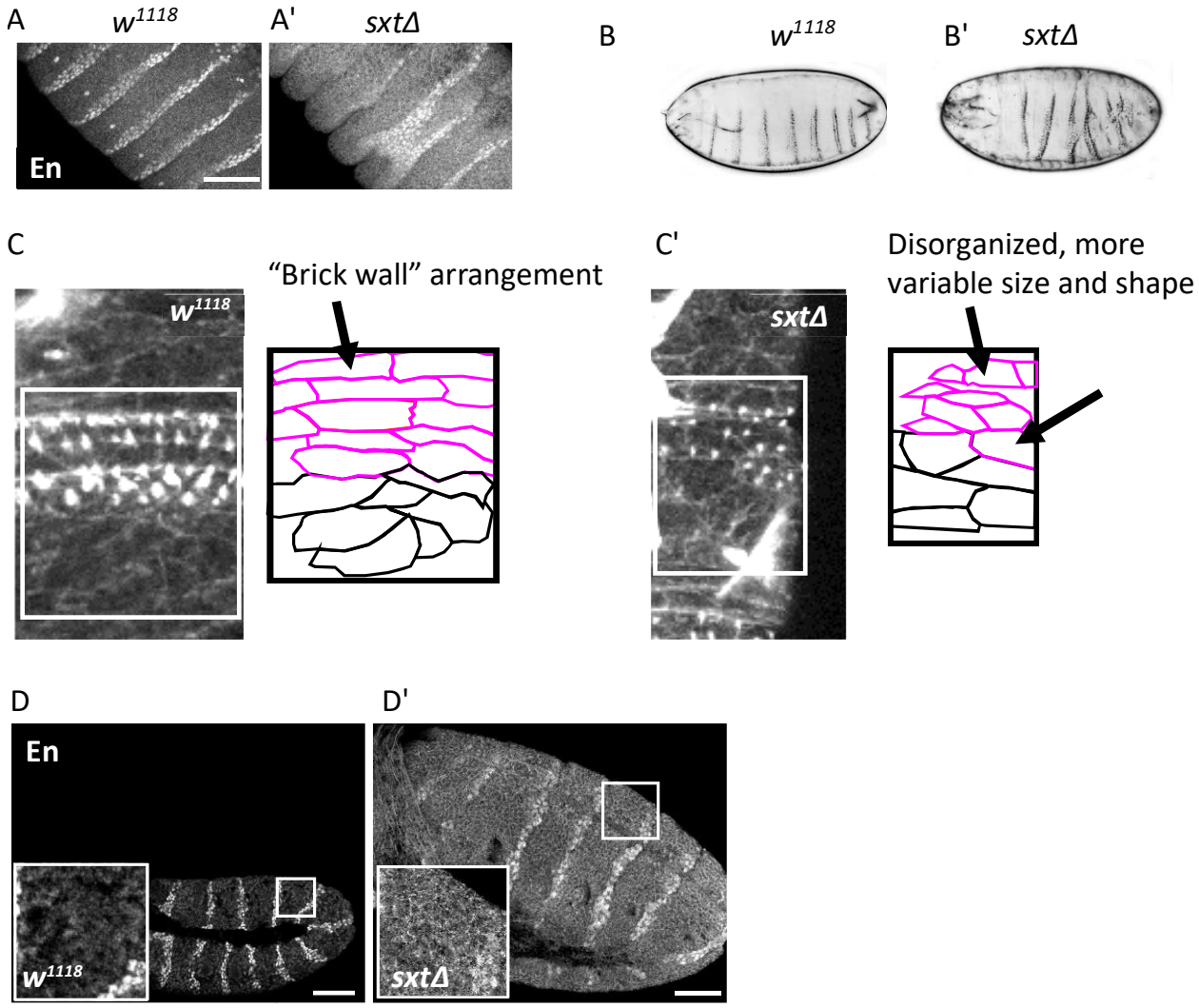

Figure S4 Segmentation defects. (A,A') Anti-Engrailed antibody marks the posterior cells in each segment in w^{1118} embryos. *sxtΔ* mutants exhibit segmentation defects. Scale bar = 50µm. (B,B') Denticle belt defects in *sxtΔ* mutants reflect segmentation defects. Lateral view (B), ventrolateral view (B'). (C,C') In Stage 16 embryos, Rhodamine-Phalloidin highlights cell cortices and the actin protrusions that secrete cuticle to form denticles (images). White squares in images show the areas drawn in the diagrams. (C) The control (w^{1118}) cells display the typical "brick wall" arrangement in the denticle-producing cells (magenta) and the larger, less organized naked cuticle cells (black). (C') Cell morphology and localization in denticle-producing cells is disrupted in *sxtΔ* mutant embryos. (D,D') Engrailed protein aberrantly localizes to cell membranes in *sxtΔ* embryos (C'), but not in w^{1118} embryos (C). White rectangle indicates area shown in close-up. Scale bar = 50µm.

1004

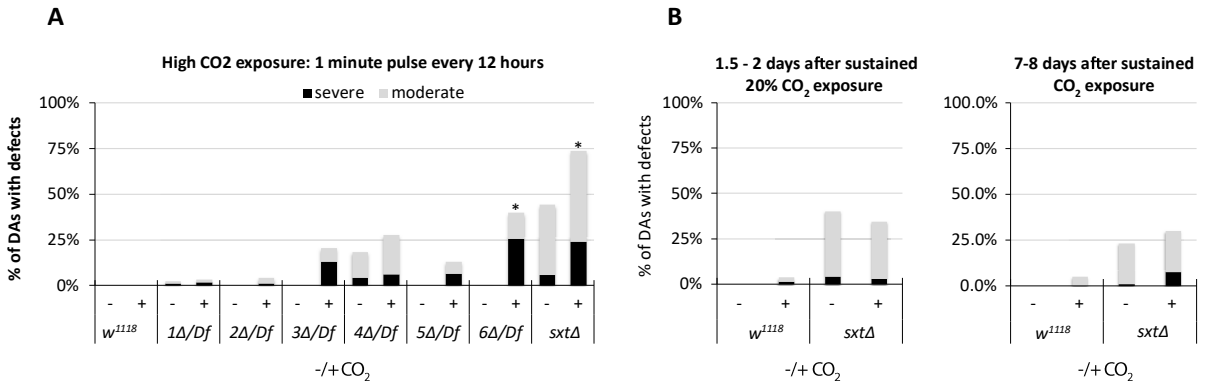

1005

1006 **Figure S5 CO_2 Exposure regimes.** DA defects are significantly increased in Idgf6Δ and sxtΔ mutants after a one-
1007 minute pulse of high (100%) CO2 exposure every 12 hours. A sustained time course of 20% CO2 for at least 1.5
1008 days and as much as 8 days does not significantly increase DA defects in these mutants. * denotes significance
1009 ($p \leq 0.05$).
1010

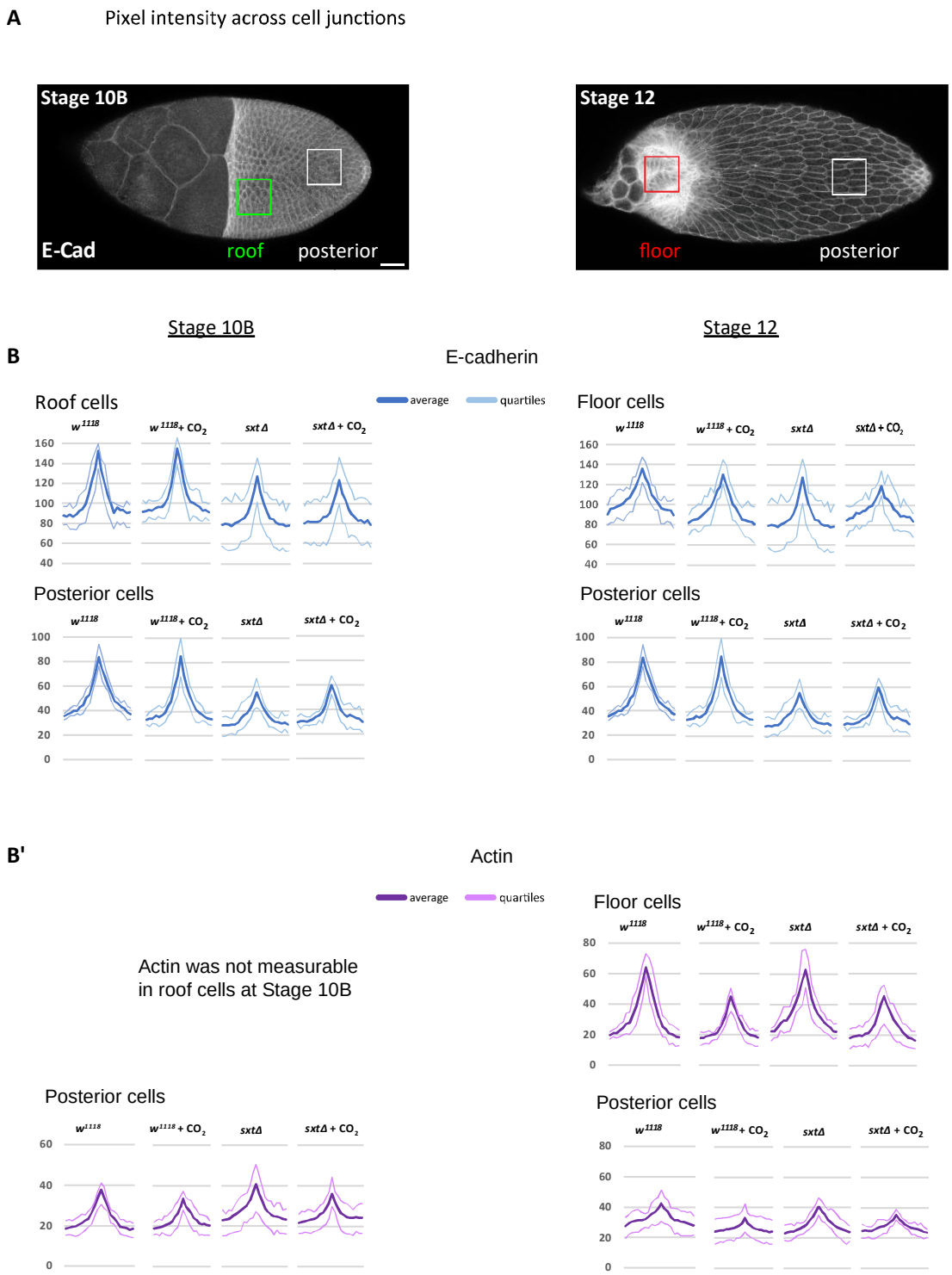

Figure S6 Quantification of cortical Actin and E-Cadherin intensity in DA cells. (A) E-Cadherin and Actin in Stage 10B roof cells (green square) and Stage 12 floor cells (red square) and in posterior columnar cells (white squares). (B) Comparison of w^{1118} and *sxtΔ* fluorescence intensity plot profiles averaged across three cell membranes, from the center of one cell to the center of the neighboring cell, averaged over at least 6 egg chambers for each genotype and each exposure regime as indicated. Plots show mean (E-cad, blue and Actin, magenta) and confidence limits (gray).

1018 **Table S1 Molecularly mapped *Idgf* gene loci, mRNA, protein lengths and weights, and deleted sequences**

Gene	Locus[a]	Length (bp)	Isoform	mRNA Length (nt)	Protein Length (aa)	MW (kDa)	Deleted Sequence[b]
Idgf1	16,445,278	1516	A	1445	439	49.4	16,445,132 - 16,446,690
Idgf2	16,447,330	3179	A	1440	440	49.2	16,449,257 - 16,450,348
			B	1796	368	41.1	
			C	1367	368	41.1	
Idgf3	16,450,907	4288	A	1649	441	49.3	16,450,962 - 16,452,978
			B	3145	441	49.3	
			C	1724	441	49.3	
			D	3801	441	49.3	
Idgf4	9,927,973	2976	A	1514	442	48.6	9,928,084 - 9,930,904
			B	1541	442	48.6	
			C	1807	442	48.6	
Idgf5	18,393,666	1617	A	1495	444	50.1	18,393,347 - 18,395,294
Idgf6	16,691,022	2730	A	1541	452	50.4	16,690,912 - 16,693,893
			B	1811	452	50.4	

1019 a. 5' nucleotide locus of molecularly mapped sequence from flybase.org
1020 b. Cas9 cuts directly before the first and after the second number
1021

1022 **Table S2 Cytological locations, gRNA sequences, and cut sites. Vertical line (|) indicates gRNA cut site,**
1023 **underlined nucleotides indicate PAM (located 3' to target on genomic DNA, not part of gRNA)**

Deletion[a,f]	Cytological Location	5' gRNA Target	3' gRNA Target
Single			
Idgf$^{1\Delta}$	2L: 36A	gtgaaactgtattagct | gac agg	tacttaattgaccgcag | tat ggg
Idgf$^{2\Delta}$	2L: 36A	acttggtctacggctat | gct ggg	gccccctaggttcttga | cac ggg
Idgf$^{3\Delta}$	2L: 36A	ggggttttcgtttcact | acg ggg	gaggccttttaggcacc | gaa agg
Idgf$^{4\Delta}$	X: 9A	aaactatataaattatc | aca cgg	gacgatagtaaacttta | taa agg
Idgf$^{5\Delta}$	2R: 55C	tccacacatttgccaca | aac tgg	atagtaaacgagctttc | aaa tgg
Idgf$^{6\Delta}$	2R: 53D	ggtcacacatgctgatt | ttc agg	ggtattcaattaaattg | cgt agg
Double			
Idgf$^{2\Delta,3\Delta}$	2L: 36A	acttggtctacggctat | gct ggg	gaggccttttaggcacc | gaa agg
Idgf$^{6\Delta,5\Delta}$	2R: 53D, 55C	b	b
Triple			
Idgf$^{1\Delta,2\Delta,3\Delta}$	2L: 36A	c	c
Idgf$^{4\Delta}$;*Idgf*$^{6\Delta,5\Delta}$	X: 9A; 2R: 53D, 55C	d	d
Sextuple			
Idgf$^{4\Delta}$;Idgf$^{(1,2,3)\Delta,(6,5)\Delta}$	X: 9A; 2L: 36A; 2R: 53D, 55C	e	e

1024 a. Additional null combinations may be generated by crossing or recombining the applicable null lines.
1025 b. Generated by recombination between *Idgf6*Δ and *Idgf5*Δ
1026 c. *Idgf1* guide and donor plasmids were injected into *vas-Cas9GFP*; *Idgf2Δ3*Δ embryos to preserve integrity of the
1027 neighboring gene *CG5888*
1028 d. Generated by crossing *Idgf*$^{6\Delta,5\Delta}$ to *Idgf*$^{4\Delta}$
1029 e. Generated by recombination between *Idgf*$^{1\Delta,2\Delta,3\Delta}$ and *Idgf*$^{6\Delta,5\Delta}$ followed by cross to *Idgf*$^{4\Delta}$ line
1030 f. All the lines are in a *w*^{1118} background

1031

1032 **Table S3 Deficiency phenotypes. The deficiencies delete the indicated Idgfs. Deficiency locus is heterozygous**
1033 **with wild-type Idgf(s) to test for DA defects caused by deletion of genes flanking the Idgfs within the**
1034 **deletion locus.**

genotype	associated Idgf deletions	normal	moderate	severe
w^{1118}; +/+	NA	98.4%	1.5%	0.1%
w^{1118}; +/Df(2L)ED1102 (VENKEN *et al.* 2006)*; +*	1Δ, 2Δ, 3Δ	99.1%	0.7%	0.1%
w^{1118}/Df(1)ED6989 (VENKEN *et al.* 2006)	4Δ	100.0%	0.0%	0.0%
w^{1118}; +/Df(2R)BSC337; +	5Δ	99.8%	0.2%	0.0%
w^{1118}; +/Df(2R)6064; +	6Δ	98.0%	2.0%	0.0%

1035